Ore mineralogy and fluid inclusions constraints on genesis of the Muteh gold deposit (western Iran)

Behzad Mehrabi[1], Ebrahim Tale Fazel*[1], Maryam Shahabifar[2]
[1] *Department of Geology, Faculty of Science, Tarbiat Moallem University, Tehran, Iran*
[2] *Iranian Mineral Processing Research Center (IMPRC)*
**Corresponding author, e-mail: fazel_tale@yahoo.com*
(*received: 29/08/2011 ; accepted: 10/05/2012*)

Abstract

The Muteh gold deposit (NE of Golpaygan) in the central part of intrusive-metamorphic belt of Sanandaj-Sirjan zone comprises NW-SE trending gold-quartz vein occurred in metamorphic complex. Gold mineralization is associated with quartz veins that formed during regional deformation across the mylonitic zones in metamorphic rocks of predominantly meta-volcanic, gneiss and schist. The sulfidation (pyritization) and silicification hydrothermal alteration as the main alteration adjacent to ore body and the quartz-sulfide veins with sulfide content of variable from 10 to 60% is dominated by pyrite, chalcopyrite, emplectite, arsenopyrite and minor content of galena and sphalerite. Native gold in the quartz veins occurs as the inclusion in pyrite and chalcopyrite and fracture fillings within pyrite. Pyrite of the late assemblage (py2) shows a range of 0.03 to 0.31 wt.% Au and 0.00 to 0.26 wt.% As and chalcopyrite have content of Au (up to 0.30 wt.%), As (up to 0.12 wt.%), and Hg (up to 0.15 wt.%) were detected in chemical composition.

Fluid inclusion (FI) shows that three types of FI include CO_2-rich or carbonic FI have homogenization temperatures of CO_2 (average 19.9°C), aqueous-carbonic FI (average salinities of 7.4 wt.%NaCl eq. and Th_{total} of 297.7°C) and aqueous FI (average salinities of 8.65 wt.% NaCl eq. and Th_{total} 254.9°C) belongs to in auriferous quartz-sulfide veins.

Evidences of metaluminous and subalkalic granitoid intrusive rocks, occurrences of albite and/or k-feldspar associated with orebodies, low sulfide content of ore mineralogy, reduced metal distributions of Au-Bi±Te±As accompanied with carbonic hydrothermal fluids, shows that gold mineralization in the Muteh, lesser or more similar to intrusion-related gold systems.

Key words: *Gold-quartz veins, Hydrothermal alteration, Intrusion-related deposits, Muteh, Iran*

Introduction

Basements rocks of western Iran consist of Paleozoic to Tertiary metamorphic rocks and late Mesozoic ophiolite mélange, comprising metasedimentary and various igneous rocks (Fig. 1). These basement rocks are cut by granitic and granodioritic intrusive bodies (e.g., Alvand batholite and granitoid complex of Boroujerd), and are overlain mainly by calc-alkaline and minor alkaline volcanic rocks. The Muteh area comprises both eastern and western metamorphic complex that the main shear zone-hosted gold-quartz vein deposit and gold occurrences occurs in the eastern part of metamorphic complex in north of the village of Muteh (Moritz *et al.,* 2006) (Fig. 2).

Initial exploration took place between 1995 by detailed geologic studies, geochemical and geophysical surveys, and drilling. Presently the Muteh gold mine consist of ten gold deposits/occurrences including two main ore zones, Chah-Khatoon and Senjedeh open pits, and eight smaller mineral occurrences (Fig. 2). It has a current total reserves of about 1.7 Mt grading 2.8 g/t at Chah-Khatoon and of 1.7 Mt grading 2.5 g/t gold at Senjedeh (Farhangi, 1991; Moritz *et al.,* 2006). The Muteh mine situated in the Golpaygan district of central Iran in central part of the Sanandaj-Sirjan metamorpho-plutonic belt in Zagros mountains (Fig. 1). The northwest-trending Zagros orogen resulted from Cretaceous and Tertiary convergence between the Eurasian and the Afro-Arabian plates and constitutes a link between the European Alpine and the Pacific systems if the Tethyan Eurasian metallogenic belt (Jankovic, 1977; 1997). The Zagros structural zone comprises the main suture units: folded Zagros in the southeastern part of the Zagros, the high Zagros, and following to northeast the Sanandaj-Sirjan zone (SSZ). The SSZ has been formed in the late Cretaceous during the closure of the Neo-Tethys and the subsequent collision of the Arabian-with the Iranian plate. The Muteh mine area was almost entirely confined to a series of steeply-dipping ductile to brittle shear zones and occurred in the Sanandaj-Sirjan metamorpo-plutonic zone. Foliated rocks and faults within the greenschist-amphibolite metamorphic belt of the SSZ host a number of orogenic-type affinity gold belt, which includes the Qabaqloujeh and Kervian occurrences, and Qolqoleh and Zartorosht deposits (Kouhestani *et al.,* 2005; Aliyari *et al.,* 2009) (Fig. 1a). The area was involved in the Cretaceous-Tertiary continental collision between the Afro-Arabian continent and the

Iranian microcontinent (Alavi, 1994; 2004; Mohajjel and Fergusson, 2000; Ghasemi and Talbot, 2005; Aliyari *et al.,* 2009). Gold mineralization is associated with quartz veins that formed during regional deformation across the mylonitic zones in metamorphic rocks of predominantly meta-volcanic, gneiss and schist.

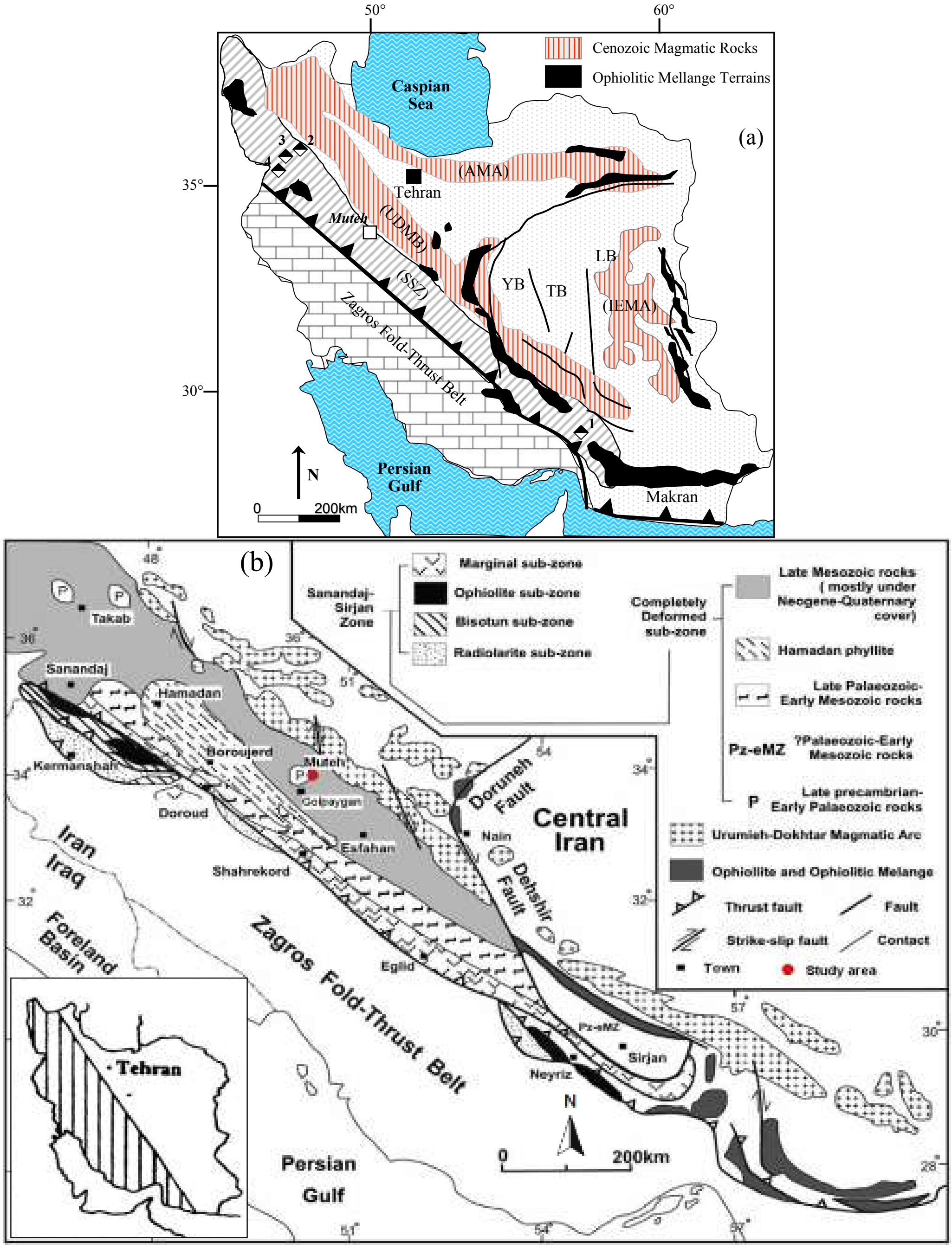

Figure 1: (a) major magmatic and structural zone of Iran (after Haghipour &Aghanabati, 1985) and location of orogenic-type affinity gold deposits (1, Zartorosht and 4, Qolqoleh) and occurrences (2, Qabaqloujeh and 3, Kervian) along the SSZ. (b) tectonic sketch map of western Iran (after Mohajjel *et al.,* 2003) showing location of the Muteh mine area and subdivisions of the Sanandaj-Sirjan tectonic zone. Abbreviation: AMA: Alborz Magmatic Arc, UDMB: Urmia-Dokhtar Magmatic Belt, IEMA: Iranian East Magmatic Assemblage, SSZ: Sanandaj-Sirjan Zone, YB: Yazd Block, TB: Tabas Block, LB: Lut Block.

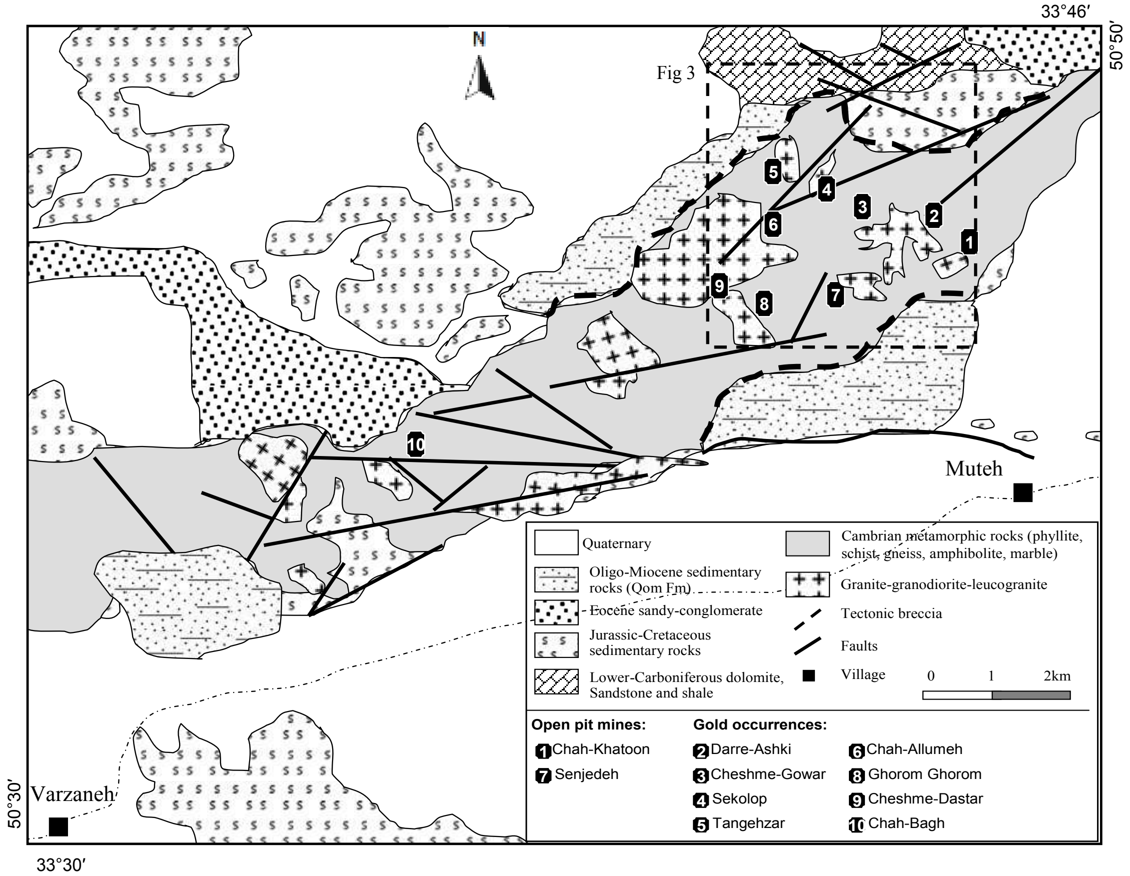

Figure 2: Simplified geologic map of the Muteh area (after Thiele *et al.,* 1968, Rachidnejad-Omran *et al.,* 2002).

Genesis, stages of development and relationships with magmatic intrusions are subjects that remain controversial for Muteh gold deposit. This fact has at attracted- and continues to attract- numerous authors. Thiele (1968) and Samani (1988) assumed that gold mineralization in the Muteh was linked to the hydrothermal activity that accompanied emplacement of development of Precambrian granitoids intrusions. A direct link between metamorphic fluids and gold mineralization as discussed by Paidar-Saravi (1989) and some authors favor either a combined meteorite-magmatic origin (e.g., Abdollahi *et al.,* 2007) for these fluids. Rachidnejad-Omran *et al.,* (2002) suggested a Paleozoic exhalative hot-spring model for generation of Muteh gold deposit. Kouhestani (2005) suggested a genetic and spatial link between gold mineralization and ductile-brittle shear zone that crosscut the metamorphic basement rocks. Moritz *et al.,* (2006) suggested that gold mineralization at the Muteh is of different ages and occurred during or after late stages of Eocene brittle extension as a result of exhumation of the host rock, during magmatic evolutions in the area.

Although the Muteh gold deposit was extensively studied in several times using traditional field and laboratory methods, the genesis of the ore body and physico-chemical condition of ore fluid has still not been satisfactorily explained. This paper presents new mineral chemistry data, and fluid inclusion study, that were collected from the Chah-Khatoon and Senjedeh open pits. New and published data in this study are used to determine the origin of the ore-forming fluids and to infer the ore-forming fluid evolution, the spatial and temporal relationship between magmatism and gold mineralization, and to compare the characteristics of the auriferous quartz veins with those of orogenic and intrusion-related deposits. The results presented in this paper have implications for the genetic models of the Muteh gold and auriferous quartz vein systems and may be a useful guide for the exploration of similar gold provinces.

Geological setting of Muteh mining area

The Muteh mine area is underlain mainly by metamorphic (i.e. marble, gneiss, amphibolite, quartzite and hornfels), pelitic metasedimentary rocks (i.e. quartz-biotite-sericite schist, quartz-chlorite-biotite schist, quartz-chlorite-albite schist), leucogranites and metavolcanic rocks (i.e. rhyolitic, andesitic tuff and lava) (Fig. 3). These rocks display variable degrees of hydrothermal alteration depending on the proximity to the mineralized shear zone. The metasedimentary rocks as a predominant rock are brown to yellowish green and have a fine-grained foliated structure. The primary, metamorphic mineralogy includes quartz-biotite-muscovite-feldspar±albite±garnet±hornblend±chlorite±epidote. These rocks are locally intercalated with quartz-rich and chlotite-biotite rich bands. Along the shear zone, both brittle faulting and ductile shearing post-date the metamorphic layering. In the north and northwestern part of the mine area, the metasedimentary and granitic rocks are intruded by slightly foliated medium to coarse-grained sill like metagabbro and granite bodies (Fig. 3). This rock exhibits variable degrees of alteration approaching the mineralized shear zones. Granite bodies include range of alkali-monzogranite, granodiorite, tonalite and syenite intrusive rocks. These granite units, extensively cut by mafic dyke, microgranite, vein-aplite, and pegmatite intrusive rocks, with intrusion of mafic rocks and schist fragments and is composed essentially of quartz, biotite, microcline, oligoclase, ±muscovite, with accessory zircon and sphene within and adjacent to the mineralized shear zone, granite suffered intensive silicification and sulfidation, subordinate sericitization and kaolinitization.

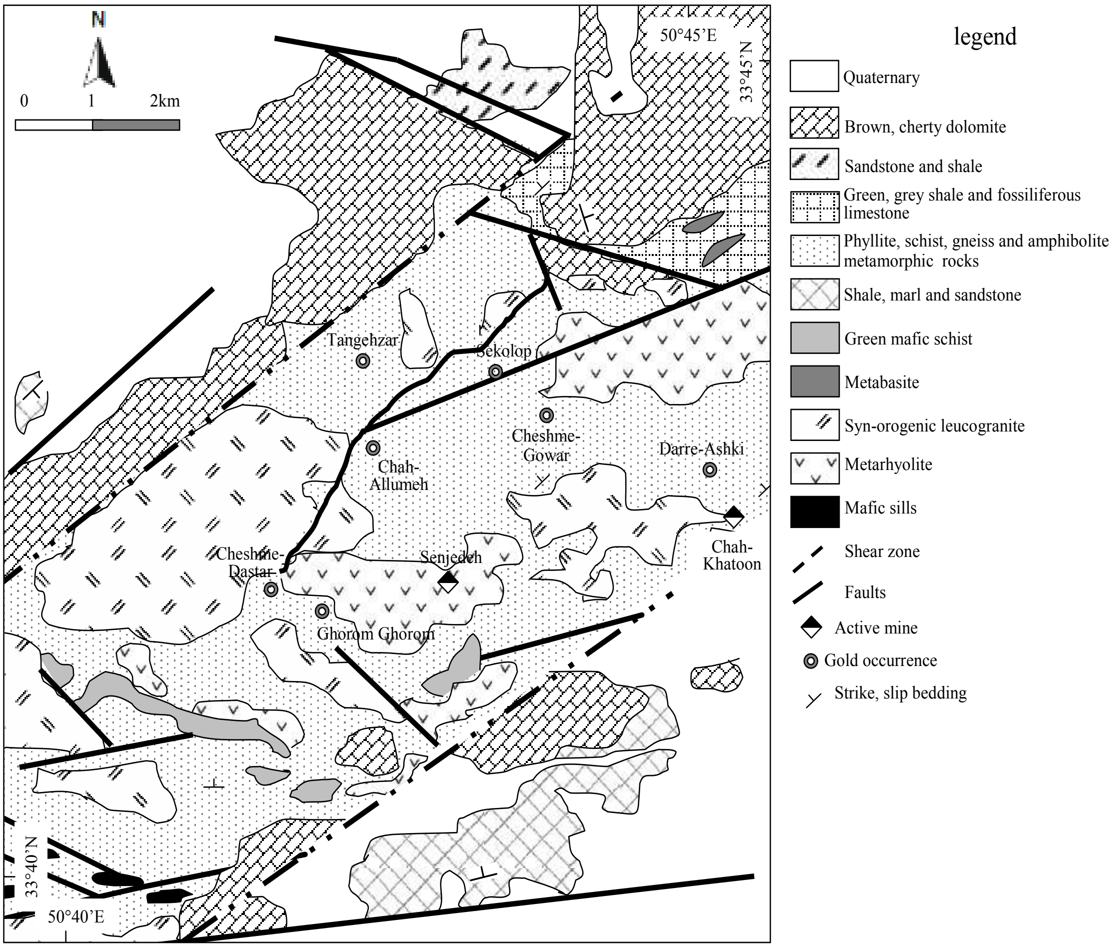

Figure 3: Geological map of the Muteh gold mine area.

Structural geology

As a part of the central Sanandaj-Sirjan metamorpho-tectonic zone, the Muteh mine area has experienced a multi-stage deformation history characterized by several overprinted folding, transpression and faulting events (Figs. 2 and 3). A summary of the structural evolution of the Muteh mine area and metamorphic basement is given in Table 1.

The metamorphic rocks display a mylonitic foliation with a NE-oriented stretching lineation within the plane of foliation (Fig. 4). They exhibit abundant asymmetric and symmetric microstructure folds and faults and shear zones at different scales. These rocks have a well-developed penetrative S_2 foliation (N45-55W/60-80°NE), axial planar to F_2 folds. This fabric is defined by preferred alignment of biotite and chlorite flakes (Fig. 6a). In the quartz-feldspatic units, the foliation is characterized by preferred orientation of quartz and alkali-feldspar defining mineral stretching lineation. S_2 foliation is overprinted by WNW-trending crenulations cleavage and its related S_3 foliation (Figs. 4 and 5a). The latter varies from an intense mineral foliation overprinting and transposing S_2 to a spaced cleavage foliation mainly in the hinge zones of folds.

Table 1: Summary of the deformation, metamorphic and magmatic event sequence of the central part of the Sanandaj-Sirjan zone (SSZ) from Mohajjel *et al.,* (1997), Golonka, (2004).

Deformation	**Fabrics**	**Metamorphic**	**Magmatism**
D_3: Formation of ductile to ductile-brittle deformation due to early Tertiary uplifting of SSZ 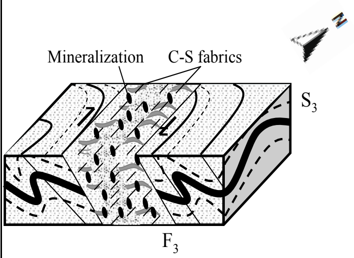	Ductile (NW-SE) and brittle (NE-SW) shear zone, locally associated with C-S fabrics, mica-fish structures and pressure shadows S_3 (NW-SE) crenulation cleavage and king band fabrics, coaxial with F_3 axial planes	Retrograde metamorphism (M_3) with development of actinolite-chlorite assemblages and rock fabrics point out to low grade, greenschist facies metamorphic overprinted the peak metamorphic fabrics	
D_2: NW-SE shear zone due to oblique collision of the Afro-Arabian continent with the southwestern part of SSZ 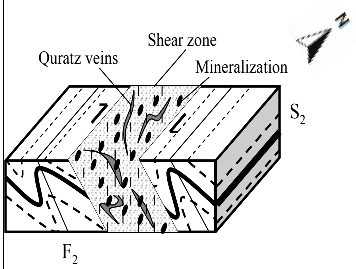	NW-SE dextral normal faults, commonly with a dextral sense of shear zone Stretched biotite and rotated of plagioclase porphyroclasts Penetrative slate foliation (S_2) striking roughly NW-SE accompanied with asymmetric upright folds (F_2).	Contact metamorphic (M_2) at the result of emplacements of intrusive bodies and development of garnet-hornblend-stuarolite phonocrysts under amphibolite facies conditions	Emplacement of syn-orogenic granitoids intrusive bodies in late Cretaceous-Tertiary
D_1: Tectonometamorphic evolution of SSZ in late Jurassic-early Cretaceous 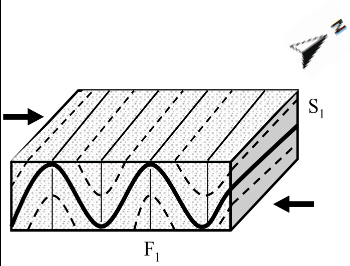	Major thrust faults led to juxtaposition of rocks from different crustal levels, related to subduction that occurred along the northeastern active continental margin of Neotethys Mesoscopic folds (F_1), axial planar schistosity (S_1) and microscopic folds Differentiated of mafic and felsic minerals	Dynamothermal (progressive) metamorphism (M_1) related to Mesozoic orogenic evolution indicated by chlorite-garnet-k-feldspar±magnetite assemblages in the pelitic metasediments	

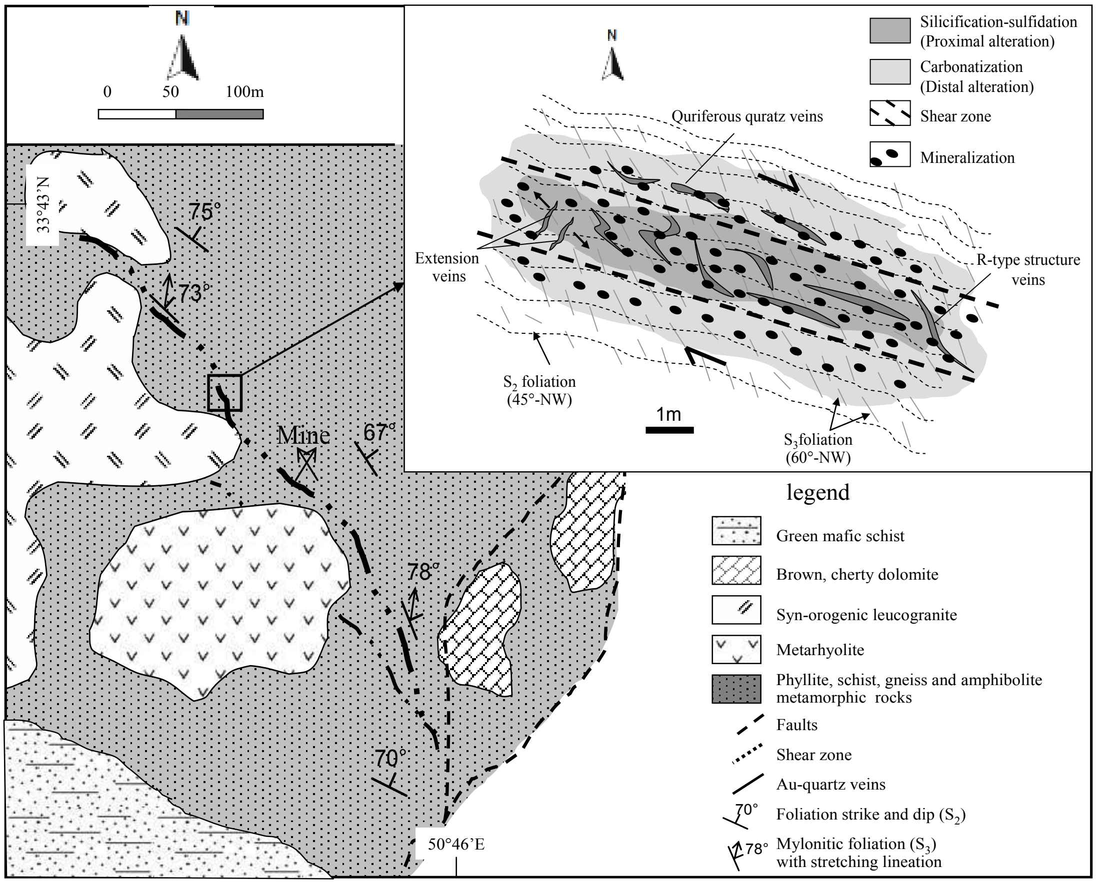

Figure 4: Sketches illustrating the geometry of the gold mineralization shear zone accompanied with alteration, Au-quartz veins and structural elements in the Chah-Khatoon open pit. In the *inset*, the synthetic structure (R-type veins) cut the foliation and occurred at the result of continuous shearing and deformation with a dextral shear sense.

Based on structural investigations, the mine area is cut by several faults with different directions. These faults which are comparable with regional ones are NW-SE, E-W and NE-SW and observed from outcrop to microscopic scales (Fig. 5b). Among them, dextral NW-trending faults, is the main structural trend and attributed to second D_2 ductile deformation increment. These faults, is parallel to ductile shear deformation, alteration and mineralization zones. NE-and EW-trending faults are also abundant in the mine area and overprint the NW-oriented structures. According to Kouhestani (2005), in the Chah-Bagh deposit, the maximum gold concentration with NW dipping lenticular shape occurred along the 40-50°NE-trending ductile shear zone. The second type of gold orebodies occurred in brittle shear zones along 40-45°NW trending, NE-dipping normal faults (Fig. 5c). Also in the Chah-Khatoon and Senjedeh open pit mine the gold-bearing quartz carbonate veins are confined to the ductile to brittle-ductile shear zone with strike of N26-37W/~60-70°NE, and 250 cm wide at average and N38-46W/30-40°NE, and 100 cm wide at average, respectively (Fig. 5d).

This shear zone is characterized by intense fracturing, asymmetric shearing and NE-stretching lineation development. Grain size reduction, sub-grain development in quartz and feldspar, mylonitic foliation and strain shadows collectively imply ductile deformation, whereas local brecciation and abrupt displacement of markers in the wallrock of shear zone denote brittle deformation (Fig. 6).

Quartz veins occurrence

The ore zone of Muteh mine area, are manifested by generally various quartz veins type and lenses along dilatant parts in the shear zones, commonly where dragging or mashing of the foliated and extension of metamorphic host rocks is observed, and/or along the contact between metamorphic basement and granodiorite rock.

At least two main types of auriferous quartz vein with different directions have been observed at Muteh, noted as types I and II, with attention to chronological sequence. Generally, most of the quartz veins cut through the metamorphic and granodiorite rocks. The gold-bearing quartz accompanied with pyrite and chalcopyrite minerals confined to the sheared zones metarhyolite rocks and adjacent to altered granite masses.

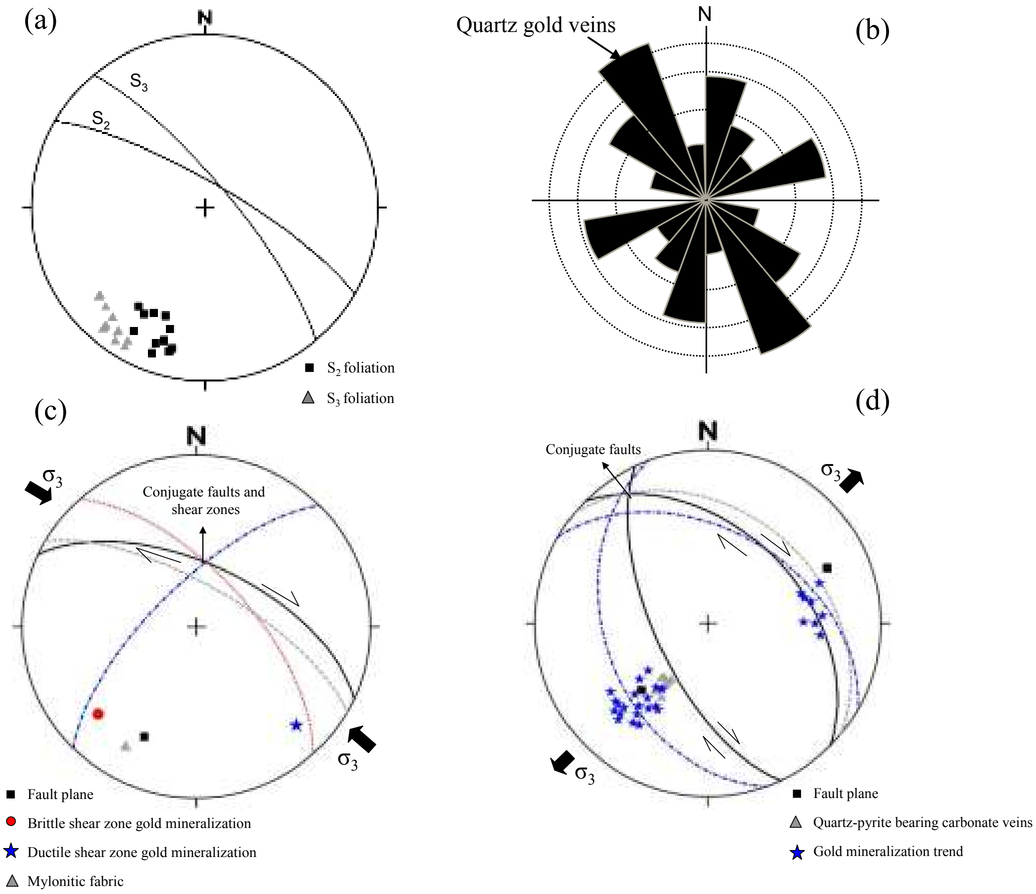

Figure 5: Stereographic plots of structural data of mineralized shear zones and quartz veins at the Muteh mine. (a) equal area projections of poles to planes of S_2 and S_3 foliations in the host metamorphic with mean great circles; (b) rose diagram of azimuths of the different fractures and main quartz gold veins encountered in the Muteh mine; (c) stereographic projection of poles to planes of brittle and ductile conjugate shear zones, mylonitic fabrics, faults accommodating the Au-quartz mineralization with mean great circles at Chah-Bagh deposit (after Kouhestani, 2005); (d) stereographic plots of poles to planes of quartz-sulfide carbonate veins (type 2) and conjugate fault systems accompanied by gold mineralization at Chah-Khatoon open pit.

Type I quartz veins contain pyrite, chalcopyrite, Cu-Bi sulfide (emplectite), pyrrhotite, arsenopyrite, electrum and marcasite with albite and k-feldspar as gangue mineral assemblages and occurred within a conjugate NW-trending normal dextral fault system dipping in opposite directions that more or less parallel to the host shear zone in the Chah-Khatoon and Senjedeh mine. According to Kouhestani (2005) in the Chah-Bagh deposit, auriferous quartz veins comprises of pyrite, chalcopyrite, arsenopyrite, covellite, digenite, Fe-oxides, malachite and azurite mineral assemblages occurred along the NW-trending reverse dextral ductile shear zone (Fig. 5c). The mineral assemblages of calcite, sulfide mineral, sericite, kaolinite and muscovite are locally common in zones of intense fracturing and brecciation and accompanied with auriferous quartz veins. Quartz veins are mainly dilated, composed essentially of coarse-grained quartz, with comb, pseudoacicular and flamboyant textures and k-feldspar porhyroclast. (Yousefinia, 2004) (Fig. 6b). The metarhyolite and siliceous sulfide bearing rocks peripheral these veins are highly bleached varying from a few centimeters to meters in width and the main lithologies for orebodies.

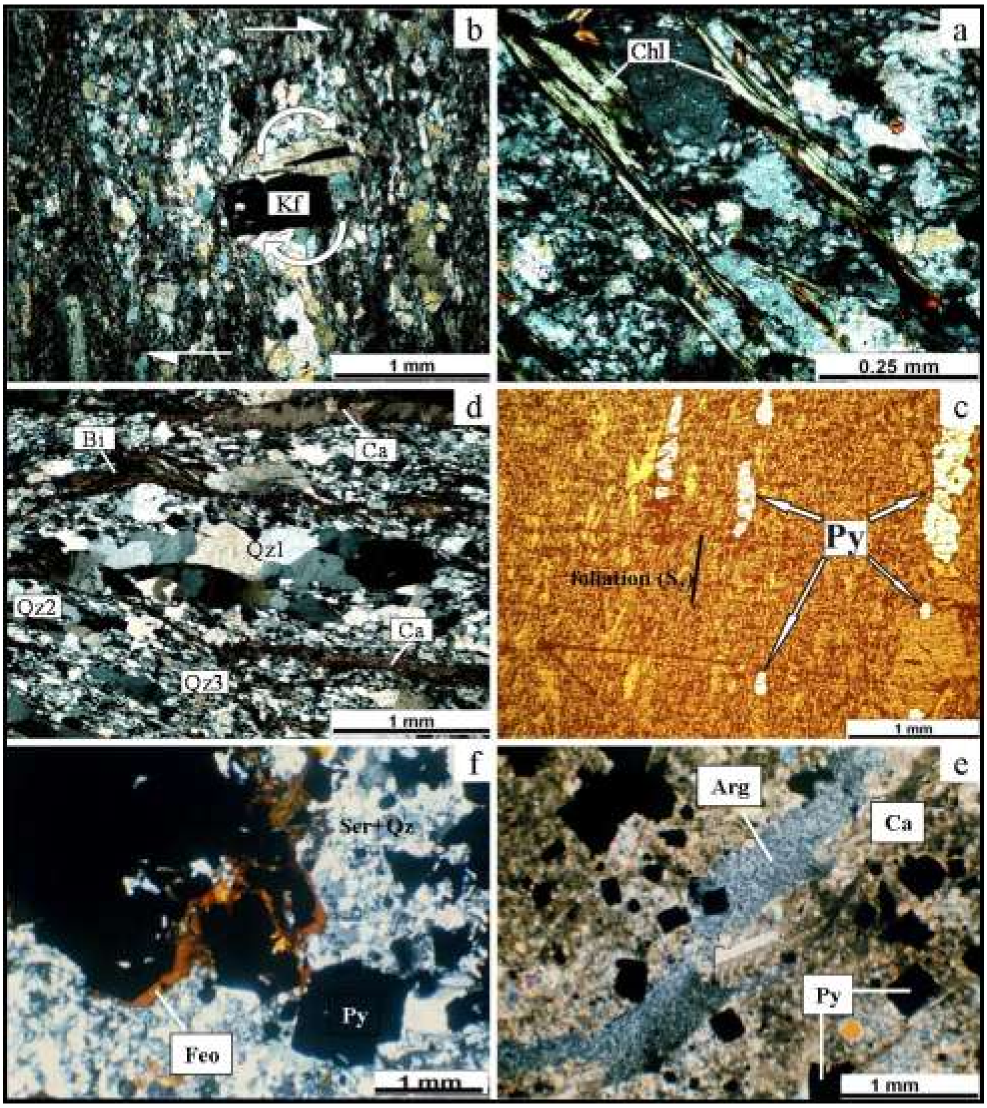

Figure 6: Photomicrographs (transmitted light) of ore fabrics and alteration assemblages in the Muteh gold deposit. (a) chlorite minerals along mylonitic shear zone; (b) clockwise rotation of a k-feldspar porhyroclast during ductile deformation, notice the dextral sense of shear; (c) euhedral to subhedral pyrite crystals in or immediately next to the quartz sulfide veins and occurred along the mylonitic foliation (S_2); (d) sheared quartz vein associated to three generations of Quartz, calcite veinlets and biotite flakes; (e) kaolinite accompanied with pyritization (cubic pyrites) and carbonate minerals in quartz-pyrite carbonate veins; (f) pervasive sericitic+quartz alteration in quartz-sulfide-gold veins with euhedral pyrite and Fe-oxide minerals. Abbreviations: Py-pyrite; Chl-chlorite; Qz-quartz; Ca-calcite; Bi-biotite; Kf-alkali-feldspar; Arg-argilic; Ser-sericite; Feo-Fe-oxide.

Type II quartz-pyrite-carbonate veins commonly occurred in the Chah-Khatoon open pit and accompanied with silicified rocks and rich in empty or limonite-filled vuges especially near the surface. These veins extend in a N40-50W direction in opposite dipping and composed essentially of quartz, carbonate, pyrite containing hydrothermal muscovite emplaced in silicified rock. The vein records open-space growths, with subhedral to euhedral quartz crystals arranged in a comb texture and have large irregular subgrains (Fig. 6d). The post-mineralization stage involved the filling of secondary fractures and voids by regional or barren quartz veins and calcite veinlets with minor late pyrite, malachite and Fe-oxide secondary minerals.

Mineralization style and hydrothermal alteration

Mineralization at the Muteh mine area is controlled by a combination of structural, alteration and deformation factors. Local studies show that veins and their gold-bearing sulfide assemblage are associated with and deformed by a major phase of NW-SE shear zone, which corresponds with regional D_2 deformation. The ore mineralization in various deposits of Muteh gold mine is controlled by a NW-SE trending, moderate to steeply dipping (NE) mylonitic shear zone and dextral fault zone and is hosted by felsic and mafic metavolcanic rocks. The maximum gold concentration (2.58 ppm) occurs in lenticular quartz bodies within 2-3 km long, 200-400 meter-wide NW-SE trending (N30-60E) ductile and brittle shear zone (Yousefinia, 2004) (Fig. 4). At least two mineralization age includes, late Cretaceous-Paleocene (56 and 68 Ma) (Rashidnejad-omran *et al.,* 2002) and Eocene (55.7 and 38.5 Ma) (Moritz *et al.,* 2006) with used of $^{40}Ar/^{39}Ar$ analytical method to be considered for Muteh gold mineralization. The gold mineralization and hydrothermal alteration occurs at least in two different styles. (1) The richest mineralization is associated with semi-massive sulfide minerals includes euhedral to subhedral pyrite, chalcopyrite, and arsenopyrite in the highly bleached metarhyolite and various type of metamorphic rocks. (2) The second style of mineralization is characterized by abundant quartz-sulfide veins that crosscut various lithological units and occurred parallel to ductile to brittle shear zone systems. Pyrite is the dominant opaque mineral and is the major phase associated with gold. Chalcopyrite, marcasite, bismuth, emplectite, arsenopyrite and pyrrhotite are subsidiary phases. The mineralized zone is parallel to S_2 deformation and restricted to deformed and hydrothermaly altered metavolcanics rocks and quartz-chlorite-sericite schists.

Hydrothermal alteration, including silicification, sulfidation, sericitization, carbonatization, and less commonly kaolinitization and chloritization, is widely developed in the NW-trending shear zones and faults and its intensity progressively increases towards the gold orebodies. The alteration mineralogy, replacement textures and destruction of metamorphic minerals indicate a low-temperature metamorphic assemblage. The mineralogical composition and intensity of the alteration are dependent on the host rock composition and indicated lateral zoning toward orebodies. This zoning is graditional and characterized by silicification and sulfidation proximal to the shear zone and ore, through a zone of sericitization-carbonization grading into a distal zone of chloritization. Silicification and sulfidation (pyritization) are observed in the inner part of the highly deformed shear zone coincident with the ore-bearing zone. Spatially, this relationship is distinguish by overprinted alteration and deformation zone and high gold grades are found in silicified, highly-deformed mylonitic and ultramylonitic metarhyolite rocks, quartz-chlorite-biotite schist rocks and in silicified sulfide-bearing veins and veinlets within the inner parts of alteration zones (Fig. 7) and (Table 2). Also, a halo of bleaching and abundant disseminated pyrites minerals observed near the type II quartz-pyrite carbonate veins (Fig. 6e), whereas, sight quartz+sericite characterizes zones accompanied with coarse pyrites bearing gold adjacent to the type I quartz-gold veins (Fig. 6f).

Ore mineralogy and mineralization style

Macroscopically, the mineralized zones are grayish-black in appearance and seem to represent tectonically produced dilatant features filled with vein-type gold ores. They range in width from 0.5 cm to 2 m and appear to be confined to a sequence of chlorite, sericite, muscovite, and quartz-chlorite-albite-sericite schist. Compositionally, the quartz-sulfide bearing gold consists mainly of medium-to coarse grained quartz interbeded with quartz-carbonate veinlets (Fig. 6d). The veins consist of weakly strained anhedral to subhedral sulfide ore-coated quartz grains containing abundant fluid inclusion and moderate solid inclusions that include some of the sulfide ore minerals. In places, the grains exhibit extension, deformation and recrystallization, implying ductile deformation. Sulfides from individual fine to medium grains occupying interstitial positions between the quartz grains and includes pyrite, chalcopyrite, emplectite (Cu-Bi sulfide), arsenopyrite, pyrrhotite, galena and sphalerite representing in total between 10 and 15% of the vein constituents. Monazite (Ce and La bearing), ankerite, rutile, zircon, marcasite, bismuth and free gold occur in miner to moderate amounts.

Ore microscopy combined with the microprobe data and backscattered electron image revealed pre mineralization (stage I) silicate and opaque minerals in the wall, including plagioclase, k-feldspar, quartz, muscovite, pyrite I, and sphalerite, galena, pyrrhotite, and at least two assemblages of sulfide minerals in the mineralized both type quartz veins and wallrock, which are interpreted as distinct generations (stage II). The early generation (pre-bonanza sub-stage) includes pyrite I, chalcopyrite I, and subordinate monazite, pyrrhotite, euhedral quartz crystals and calcite minerals is common mineral assemblages in the quartz-pyrite carbonate veins (type II) as disseminated or cluster in quartz veins and veinlets. A later generation (bonanza sub-stage), dominated by auriferous pyrite II and chalcopyrite II, emplectite, arsenopyrite, pyrrhotite, and subordinate tellurium bearing minerals and native gold. This assemblage occurs commonly in the quartz-sulfide veins (type I) as disseminations or accompanied with k-feldspar and albite gangue minerals (Fig. 8). Marcasite, hematite, kaolinite, cahlcantite, gypsum and Fe-oxide minerals are disseminated in the altered wallrocks.

Table 2: Compositional variations of trace element concentrations in various types of gold mineralization host rock in the Muteh mine (ppm).

sample	Quartz-chlorite-biotite schist			Granite		Hornfels		Metarhyolite			Amphibolite
	M-70	M-279	M-106	M-25	M-206	M-332	M-319	M-368	M-317	M-148	M-316
Au	1.12	1.27	14.70	1.16	3.87	3.19	8.73	3.71	4.11	6.60	3.38
Pb	10.9	276	20.2	9.2	7.4	4	1202	20.9	16.6	52.6	13.9
Ba	93	294	65.4	564	859	538	104	238	446	247	354
Hg	0.037	0.07	0.08	0.07	0.0375	0.08	0.07	0.0375	0.19	0.06	0.06
Ag	0.22	0.6	0.72	0.06	0.65	1.04	0.15	0.1	0.08	2.41	0.66
As	10.9	212	80.7	3.1	4.3	14.9	32.8	109	23.4	93.1	14.4
Bi	8.7	0.1	1.5	0.076	0.5	1.6	0.2	0.1	0.2	2.6	1.7
Cu	19.6	71.6	117	14.9	12.4	42	26.5	148	42	153	59.2
Mo	1.5	13.4	3.9	3.6	5.1	6.2	59.3	40.2	17.1	53.2	162
Sb	0.3	1.1	2.5	0.22	0.3	0.5	1.7	2.5	1.6	0.7	0.5
Sn	1.4	1.4	1.7	3.2	3	2.4	1.4	2.3	2.9	2.7	1.6
W	1.2	2.1	0.5	2.2	2	4.5	2.5	6.7	14.8	2.8	1.6
Te	8	0.5	0.8	0.15	0.8	2.2	1.4	0.15	0.3	8.7	2.3
Zn	9.5	345	70.2	9.1	13.2	6.3	26	96.2	62.2	124	81.2
Cd	0.075	0.5	0.7	0.075	0.075	0.076	0.075	0.2	0.2	0.4	0.7
Tl	0.075	0.1	0.075	0.2	0.2	0.2	0.1	0.2	0.6	0.4	0.4
Mn	149	130	200	83	75	64	55	94	368	142	24.50
Ti	1520	842	1010	905	689	696	736	1080	2750	2900	1310
Fe	21600	26600	58800	11500	18000	15900	16600	75	39000	54800	92400
S	130	890	3920	37.5	120	170	1700	210	110	470	340
P	427	273	533	84	159	56	271	446	231	871	163
K	5600	11400	2010	25700	22800	18100	7580	9990	18900	19000	8230
Al	37800	24400	19200	78600	61300	60300	46900	64300	77800	67400	23400
Ca	3060	1730	4170	2710	5580	3330	2100	5570	12300	3870	176000
Mg	7850	2220	4510	948	619	623	2930	2170	8650	10600	2720
Na	18000	4850	8690	37000	38900	34100	33100	38200	37100	29600	8570

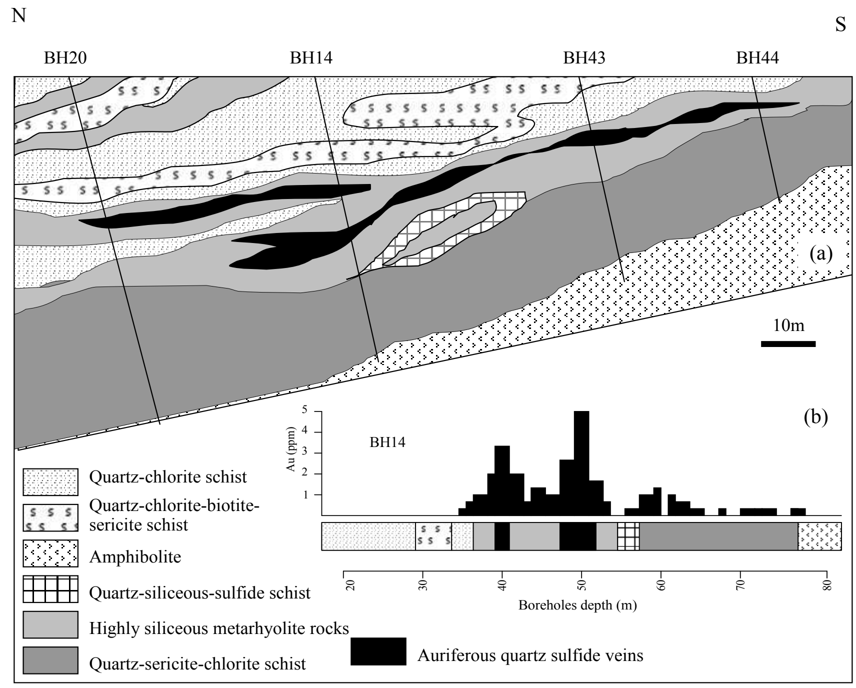

Figure 7: (a) north-south cross section, showing various part of gold hosted geometry, and (b) distribution of Au in selected cross section (BH14) from the Chah-Khatoon open pit. Data after Moritz *et al.,* (2006) and Hajizadeh (2009). Compositional variations of element in various rock types are given in Table 2.

As discussed above, pyrite is the dominate ore mineral (>50 vol.% of sulfides) and is the major phase associate with gold, commonly occurring as a two types include: (1) fine to moderate-grained, subhedral to anhedral pyrite (up to 100 µm) in the granite rocks or in metamorphic segregation quartz veins and crosscutting the foliation with a minor gold as a solid-solution phase (Table 3); (2) coarse-grained, euhedral to subhedral pyrite (up to 1 mm) in or immediately next to the sulfide-bearing quartz veins and more or less along the foliation of the host rocks and is indicative of high gold grades (Figs. 6c and 8a) and (Table 3).

Table 3: Microprobe analysis of various generations of pyrite and chalcopyrite accompanied by Cu-Bi sulfide phase, in the Muteh deposit (wt.%).

	Fe	S	Cu	Zn	As	Ag	Te	Au	Hg	Bi	Au/Ag
Py1 (13)[a] (Ave.)	47.20-48.18 47.69	52.13-53.23 52.68	0.03-0.16 0.09	0.01-0.04 0.02	0.02-0.14 0.08	0.02-0.13 0.07	0.00-0.14 0.07	0.00-0.09 0.04	0.00-0.07 0.03	------	0.57
Py2 (18)[a] (Ave.)	47.01-48.16 47.58	51.23-53.46 52.34	0.01-0.11 0.06	0.01-0.03 0.02	0.00-0.26 0.13	0.00-0.1 0.05	0.00-0.04 0.02	0.03-0.31 0.17	0.00-0.11 0.05	------	3.4
Cpy1 (14)[a] (Ave.)	30.03-30.98 30.50	34.33-35.16 34.74	33.62-34.20 33.91	0.00-0.04 0.02	0.01-0.14 0.07	0.00-0.08 0.04	0.00-0.06 0.03	0.07-0.37 0.22	0.01-0.17 0.09	------	5.5
Cpy2 (15)[a] (Ave.)	30.11-30.84 30.47	33.60-35.00 34.3	33.65-34.59 34.12	0.00-0.03 0.01	0.02-0.11 0.06	0.00-0.09 0.04	0.01-0.08 0.04	0.01-0.14 0.07	0.00-0.06 0.03	------	1.75
Cu-Bi sulfide(9)[a] (Ave.)	0.06-2.29 1.17	18.68-20.29 19.48	12.21-19.60 15.90	0.00-0.16 0.08	0.00 0.00	0.1-0.59 0.3	0.01-0.18 0.09	0.01-0.17 0.09	0.00-0.11 0.05	60.50-67.06 63.78	0.27

[a] number in parentheses indicate number of sulfide mineral grains.

Chalcopyrite as a accessory mineral after pyrite and was deposited during both stages includes: (1) disseminated anhedral fine grains (up to 150 µm) intergrown with fine-grained pyrite, and is locally abundant (up to 1%). (2) coarse grained, subhedral to anhedral, ranging in size up to 5 mm and occurs in siliceous gangue and intergrown with first-generated pyrite (Fig. 8)

Emplectite ($CuBiS_2$) is the third most abundant ore mineral after pyrite and chalcopyrite respectively, occurs in quartz-sulfide veins (type I) and coexist with pyrite, chalcopyrite, pyrrhotite, k-feldspar and albite (Fig. 8a-b). It generally occurs as a anhedral to subhedral coarse grains (up to 1 mm) and in places, the occur as aggregates in continues array probably indicating the direction of foliation during recrystallization (Fig. 8c).

Native gold and electrum occur as follow; (1) they are commonly occur as rounded inclusions enclosed by disseminated pyrite or are distributed in fractures within coarse pyrite and chalcopyrite (Fig. 8e-f); and (2) they occur as gold nugget (range in grain size between <10 to 100 µm) and/or fracture-filling in pyrite-chalcopyrite-albite-k-felspar veins (Fig. 8d).

There are, in general, three main generations of hydrothermal quartz in the mine area. First-generation quartz (Qz1) is observe in mylonite and ultramylonite schist within NW-trending shear zone, where it occurs as rotated elliptical porphyroclasts in association with early-formed pyrite (Py1). The second-generation quartz (Qz2) occurs as fine-grained hydrothermal quartz and/or sulfide-quartz veinlets associated with second-generation pyrite (Py2) and is widespread within alterad carbonaceous mylonite schist (Fig. 6d). The third-generation quartz (Qz3) occurs as within late mineralization stage quartz-sulfide veins accompanied with both type-generation pyrites (Fig. 9).

Minerals chemistry

Ore mineral chemistry has been obtained for the vein minerals, ore and gangue, of the different paragenetic phases and was determined on a CAMECA SX100 electron microprobe and a REM Leo 32-1440 scanning electron microscope at the Iranian Mineral Processing Research Center (IMPRC). The applied accelerating voltage was 20 kv, and specimen current was 20 nA. Detection limits were 0.001 wt.%.

Alteration of pyrite to Fe-hydroxide commonly observed. Based on the microprobe analysis, Au, As, Ag, Cu, Te, Hg, and Zn are the common trace elements found in selected crystals and Au is the most abounded trace element in pyrite. In order to detect any zonation within pyrite, points from grain cores and rims were analyzed. In some samples, pyrite grains are compositionally more variable than other. Pyrite of the late assemblage (py2), associated with chalcopyrite, emplectite, pyrrhotite and arsenopyrite shows a range of 0.03 to 0.31 wt.% Au and 0.00 to 0.26 wt.% As. Also, microprobe analysis indicated variation of As, Ag, Hg, and Te in chalcopyrites. Based on these analysis, high levels of Au (up to 0.30 wt.%), As (up to 0.12 wt.%), and Hg (up to 0.15 wt.%) were detected across some of these grains.

Microprobe analysis indicated variation of Cu (12.2 to 19.6 wt.%) content in emplectite grains. Concentration of Cu caused to alteration of acantite around the Cu-bearing bismuth. Other trace element compositions are Ag, Au, Zn, and Te with variation in content in emplectite. Microprobe point analysis, also shows some evidence of Au (0.01 to 0.17 wt.%), Hg, Te, Ag, Zn, and Fe association with emplectite grains and bivariant correlation between Bi-Au and Bi-Ag elements are detected (Fig. 10).

Analysis of all the three generation native gold indicate similar chemistry with minor content of Ag (0.12 wt.%). The average Au/Ag ratio of the ore is 8.5 and the content of Pb and Zn is very low. A summary of mineral chemistry is provided in Table 3.

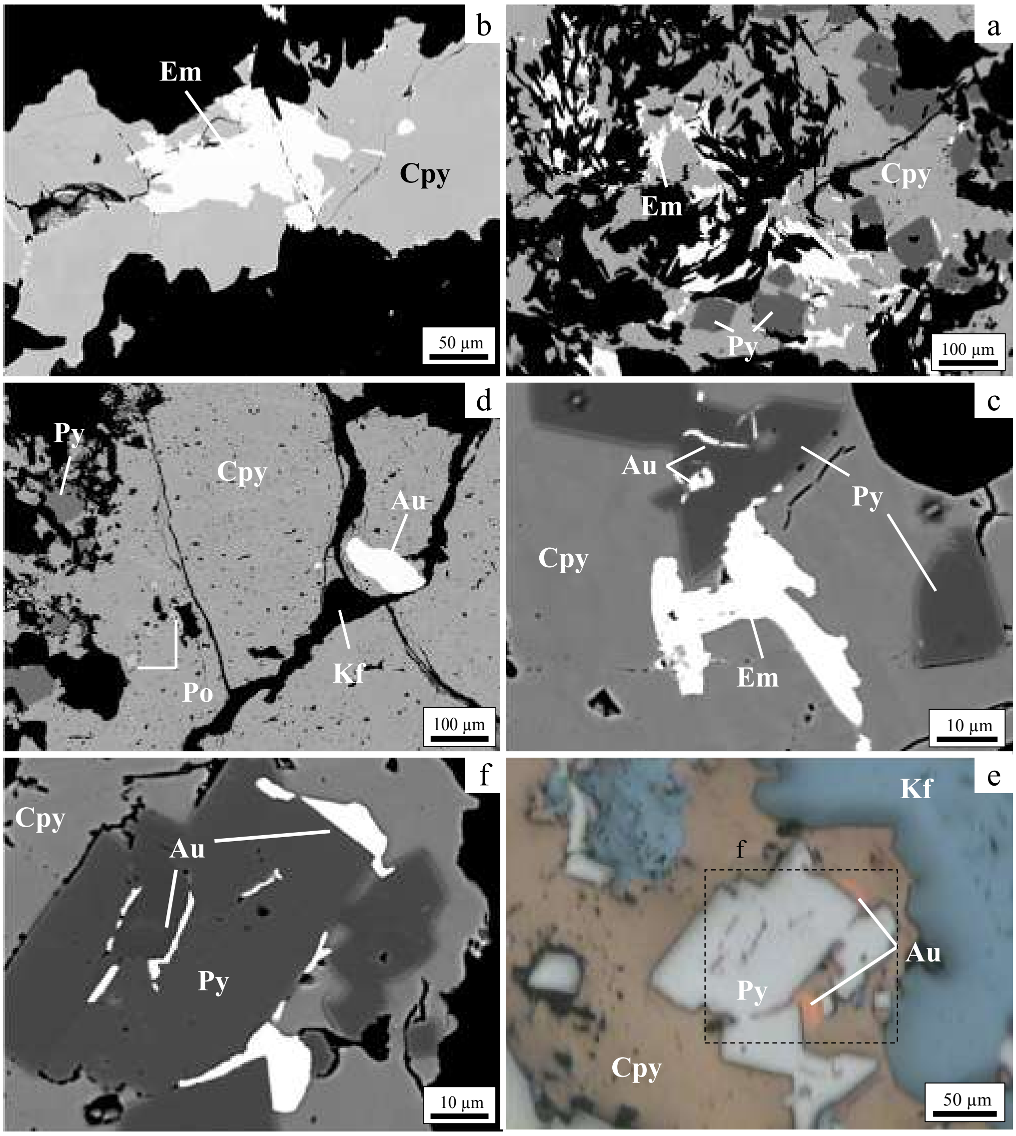

Figure 8: SEM-BSE images of assemblages in the Muteh, (a) euhedral pyrite and a late emplectite-chalcopyrite assemblage; (b) chalcopyrite and emplectite intergrown; (c) pyrite crystals associated to chalcopyrite, emplectite and occurrence of gold in microfractures pyrite crystals; (d) microcrackes in auriferous chalcopyrite healed by late k-feldspar at the margin of gold nugget (~100 µm) associated to early pyrite crystals and pyrrhotite; (e) photomicrographs of auriferous pyrite crystals (py2) associated to rounded peripheral native gold, chalcopyrite and late k-feldspar mineral

assemblage; (f) native gold commonly occur as rounded inclusions enclosed by disseminated pyrite and/or distributed in fractures within coarse pyrite and chalcopyrite. Abbreviations: Py-pyrite; Cpy-chalcopyrite; Po-pyrrhotite; Em-emplectite; Au-native gold; Kf-alkali-feldspar.

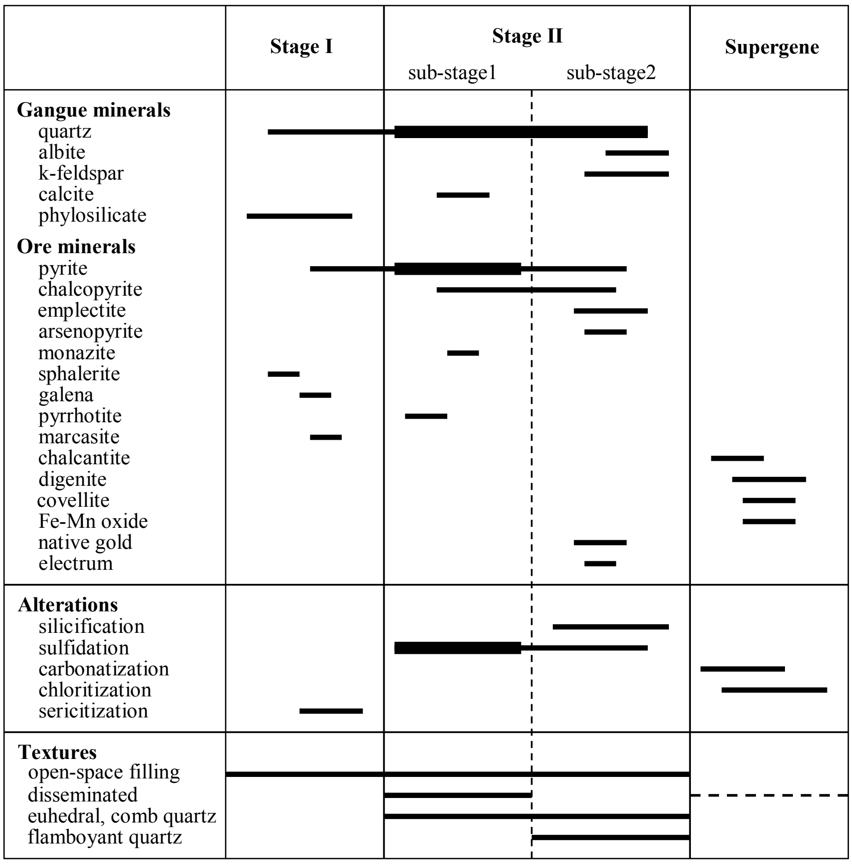

Figure 9: Paragenetic sequence ore and gangue minerals, accompanied by alteration haloes and textures in the Muteh deposit

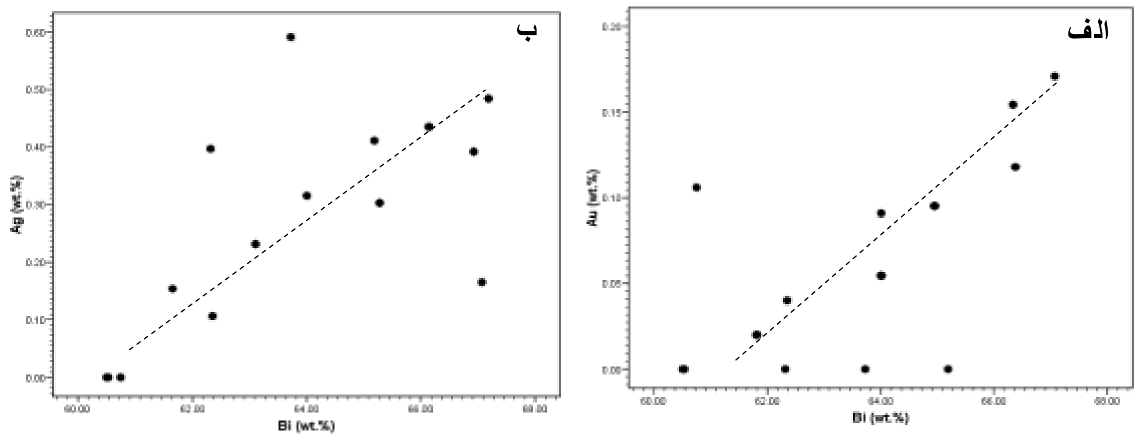

Figure 10: Bivariant correlation between (a) bismuth-gold, and (b) bismuth-silver contents in the emplectite.

Fluid inclusions

Fluid inclusion microthermometry was carried out on inclusions in vein quartz using a Linkam THM600 heating-freezing stage, fitted with a thermal control unit TMS-93 and equipped with Ziess microscope at the Tarbiat Moallem University of Iran and employing standard procedures (Shepherd *et al.,* 1985). The stages enable measurements within the range of -90°C and 550°C. Freezing and heating runs were, respectively, undertaken using liquid nitrogen and a thermal resistor calibration of the stage was carried out by using standard natural and synthetic inclusions. Molar volumes, compositions and isochores were calculated using the FLINCOR software (Brown, 1989). The salinity of aqueous fluid inclusions devoid of dissolved gases was calculated with the equation of Bodnar (2003). Salinities from final clathrate melting were based on Diamond (1992) equation.

Fluid inclusion studies aimed at assessing the nature and evolution of the mineralizing fluids and to consider the physicochemical parameters which controlled gold mineralization in regard to the regional metamorphic and magmatic framework of the country rocks in the study area. The succession of fluid has been studied by examining relationships between fluid inclusion, their host mineral, geometry of the host microstructures and location of orebodies.

Petrography and microthermometry

Fluid inclusion study was undertaken on two types quartz-vein from various parts of shear zone includes barren, regional quartz veins in metamorphic rocks and quartz from silicified host rocks from gold orebodies of the Senjedeh and Chah-Khatoon open pit (Fig. 3). Petrographic observations and heating-freezing measurements helped to define at least three compositionally different types of inclusions, includings: carbonic (CO_2 rich) inclusions, aqueous-carbonic (H_2O-CO_2-NaCl±CH_4) inclusions, and aqueous (H_2O-NaCl±$CaCl_2$) inclusions. Microthermometric data were collected from inclusions in the less deformed vein quartz. The obtained data, including temperatures of total homogenization (Th_{total}), melting of CO_2 (Tm_{CO2}), homogenization of CO_2 (Th_{CO2}), melting of clathrate (Tm_{clath}) and final melting of ice (Tm_{ice}), are summarized in Table 4. As the investigated gold-bearing quartz veins are spatially and temporally associated with a shear zone, inclusions are classified into isolated, clustered and fluid inclusions in intra-grain, inter-grain and trans-grain trails (e.g., Simmons and Richter, 1976; Touret, 1981; Kranz, 1983; Van Den Kerkhof and Hein, 2001; Zoheir, 2008) (Fig. 10).

CO_2-rich (carbonic) inclusions, approximately 45% of the whole population, range from 4 to 15 μm are defined by their lack of clathrate formation during cooling. In general, inclusions of this type are commonly oval to negative crystal shaped single (L_{CO2}) or two (L_{CO2}+V_{CO2}) phase at room temperature. These inclusions locally, they also occur with CO_2-H_2O inclusions. The origin of CO_2-rich inclusions varies from primary to pseudosecondary corresponding to the occurrences of isolated, inter-grain and trans-grain inclusion trials. These inclusions yielded Th_{CO2} to the liquid phase ranging between 12.6°C to 22.3°C, corresponding to densities of 0.82 to 0.71 g/cm^3, respectively. Generally, the final melting of CO_2 (Tm_{CO2}) occurred between -56.7°C and -58.6°C. Lowering of Tm_{CO2}, below the -56.6°C is attributed to the presence of incompressible gases, e.g., CH_4 or N_2 (Burruss, 1981).

H_2O-CO_2-NaCl±CH_4 (aqueous carbonic) inclusions, characterized by irregular or negative crystal shapes showing a random three-dimensional distribution typically throughout less deformed quartz crystals. Fluid inclusions within this group, are generally between 5 to 30 μm in size and consist of two phase (L_{H2O}+L_{CO2}) at room temperature and a third phase (L_{H2O}+L_{CO2}+V_{CO2}) appears during cooling. The degree of fill varies from 0.3 up to 0.8 (visual estimation at 25°C) within a single trial. They occur mainly as isolate, cluster and as trials but generally confined to individual quartz grains. These inclusions are generally considered as primary in origin. The final melting of CO_2 (Tm_{CO2}) ranges from -56.7 to -58.3°C. The clathrate melting temperature (Tm_{clath}) was measured between 2.5°C and 8.8°C and indicate salinities between 2.3 to 12.5 wt.% NaCl eq. Homogenization of CO_2 (Th_{CO2}) occurred commonly into liquid phase between 10.4°C and 23.7°C, implying range of 0.72-0.84 g/cm^3 and ~0.90 g/cm^3 for CO_2 and bulk densities, respectively. Upon heating of the bubble-dominated inclusions, the CO_2 bubble expanded instead of shrinking, indicating homogenization into vapour (e.g., Roedder, 1984). Generally, a range of CO_2 contents of 5-10 mol% was calculated for the examined aqueous-carbonic inclusions. Total homogenization temperature (Th_{total}) took place between 145.6°C and 304.2°C commonly into liquid. The abundance of these inclusions is directly related to silicified host rocks from gold orebodies of the Chah-Khatoon and Senjedeh open pit.

H_2O-NaCl±$CaCl_2$±$MgCl_2$ (aqueous) fluid inclusions, are commonly two phase (L+V), ranging in size from 15 to 35 μm. They occur as three-dimensional clusters, isolated individuals, inter-grain and/or trans-grain trials and very scarcely coexisting with CO_2-H_2O or CO_2-rich inclusions cutting quartz grains. They are interpreted as primary in origin and usually have a higher vapor to liquid ratio than secondary inclusions. The final ice melting temperature (Tm_{ice}) indicating two groups, includes; (1) ranging from -1.2°C to -

11.3°C (with a data peak between -4°C to -6°C) and salinities of 2.1 to 15.2 wt.% NaCl eq. for quartz-sulfide gold veins and; 2) ranging from -12.5°C to -26.7°C (with a data peak between -21°C and -22°C) and salinities of 16.4 to 28.2 wt.% NaCl eq. calculated for regional or barren quartz veins. Total homogenization temperature (Th_{total}), consistently into liquid, took place differentially within two temperature ranges, 147.4°C to 245.6°C for the intra-grain and inter-grain trial-bound inclusions of barren quartz veins, and 212.2°C to 297.6°C for inter-grain to trans-grain trials inclusions of quartz-sulfide gold veins (Table 4).

Table 4. Summary of microthermometric data from carbonic (type1), aqueous-carbonic (type2) and aqueous (type3) inclusions quartz veins. Degree of fill refers to the volumetric proportion of H_2O-rich phase estimated visually at room temperature (25°C) from charts of Shepherd et al., (1985). Mode of homogenization is recorded as *L*., to liquid. Tm_{CO2}, Th_{CO2}, Tm_{ice}, and Th_{total} refers to final melting temperature of CO_2, homogenization temperature of CO_2, final ice melting temperature, and total homogenization temperature, respectively. For type 2 inclusions, salinity is estimated from clathrate-melting temperature (Tm_{clath}).

	Type 1 *n*=30	**Type 2** *n*=42	**Type 3a** *n*=21	**Type3b** *n*=16
Degree of fill (Ave.)	0.5 to 0.7 (0.6)	0.3 to 0.8 (0.85)	0.2 to 0.7 (0.45)	0.3 to 0.75 (0.52)
Tm_{CO2} (Ave.)	-56.7 to -58.6 (-57.6)	-56.9 to -58.3 (-57.6)	---------	---------
Th_{CO2} (Ave.)	12.6 to 27.3 (*L*) (17.4)	10.4 to 23.4 (*L*) (16.9)	---------	---------
Tm_{clath} (Ave.)	---------	2.5 to 8.8 (5.6)	---------	--------
Tm_{ice} (Ave.)	---------	---------	-1.2 to -11.3 (-6.25)	-12.5 to -26.7 (-19.6)
Th_{total} (Ave.)	---------	145.6 to 304.2 (*L*) (224.9)	212.2 to 297.6 (*L*) (254.9)	147.4 to 245.6 (*L*) (196.5)
CO_2 density (g/cm^3)	0.71 to 0.82	0.72 to 0.84	---------	---------
Salinity (wt.% NaCl eq.)	---------	2.3 to 12.5	2.1 to 15.2	16.4 to 28.2

Discussion

Pressure and temperature estimation

Pressure and temperature conditions of fluid entrapment are determined from relevant isochores of two fluid systems, constructed on the basis of the equations of state of Potter *et al.,* (1978) and Zhang and Frantz (1987) and FLINCOR software (Brown, 1989). Based on the aforementioned, a CO_2-bearing fluid, as represented by coexisting H_2O-CO_2 and primary aqueous inclusions, can be taken as representive of gold associated fluids. Estimates of trapping pressure can only be obtained if the fluid inclusions were trapped under immiscible or boiling conditions or if an independent trapping temperature is known (Brown & Hagemann, 1995). Specially, trapping pressure can be approximated from end member inclusions trapped nearest the solvus if the inclusions formed in the immiscible two-phase field (Zhang *et al.,* 2005). With attention to the predominance of H_2O-CO_2 inclusions, we assume that their mean bulk composition represents the mean composition of the parent auriferous quartz vein forming fluids (Bowers & Helgeson, 1983), therefore, we selected two fluid inclusions to estimate trapping pressure based on their end member low and high CO_2 contents (Fig. 12). Inasmuch fluid inclusion bulk homogenization temperatures (Th_{total}) can only be used to provide minimum quartz-vein temperatures and pressure estimates are always difficult (Roedder & Bodnar, 1980). In this paper used the same logic as used by Fan *et al.,* (2003) and latterly Zhang *et al.,* (2005) to revise the treatment of temperature and pressure: Measured homogenization temperature are X using these as minimum temperature values. A preliminary minimum pressure (P1) can be calculated from the isochores. Using this value of P1, trapping temperatures for fluids can be estimated as X+Z. Z is a temperature calculated from pressure correction. This correction trapping temperature can then be used to calculate, the accurate pressure (P2).

Minimum homogenization temperature for H_2O-CO_2-NaCl fluid inclusions related to mineralization is 145.6°C to 304.2°C. The preliminary minimum pressure (P1) from calculated isochores (Fig. 12) is about 1.3 kbar with pressure correction of about 100°C (Roedder, 1984). Therefore, the temperature of trapping for H_2O-CO_2-NaCl fluid inclusions is from 245.6°C to 404.2°C with the recalculated trapping pressure (P2) is from 2.1 to 2.7 kbar variation in total homogenization temperature (Th_{total}), densities, and compositions of the aqueous-carbonic (type II) and aqueous (type III) inclusions might reflect the variation of the physico-chemical conditions during the mineralizing process (Schmidt Mumm *et al.,* 1997). Also, spread of the isochores and pressure data my also account for pressure fluctuations, a common fracture in the shear zone-hosted vein gold deposits, in which fluid pressure often exceeds the lithostatic conditions (Sibson, 1987; Robert and Kelly, 1987; Cox *et al.,* 1995; Zoheir, 2008).

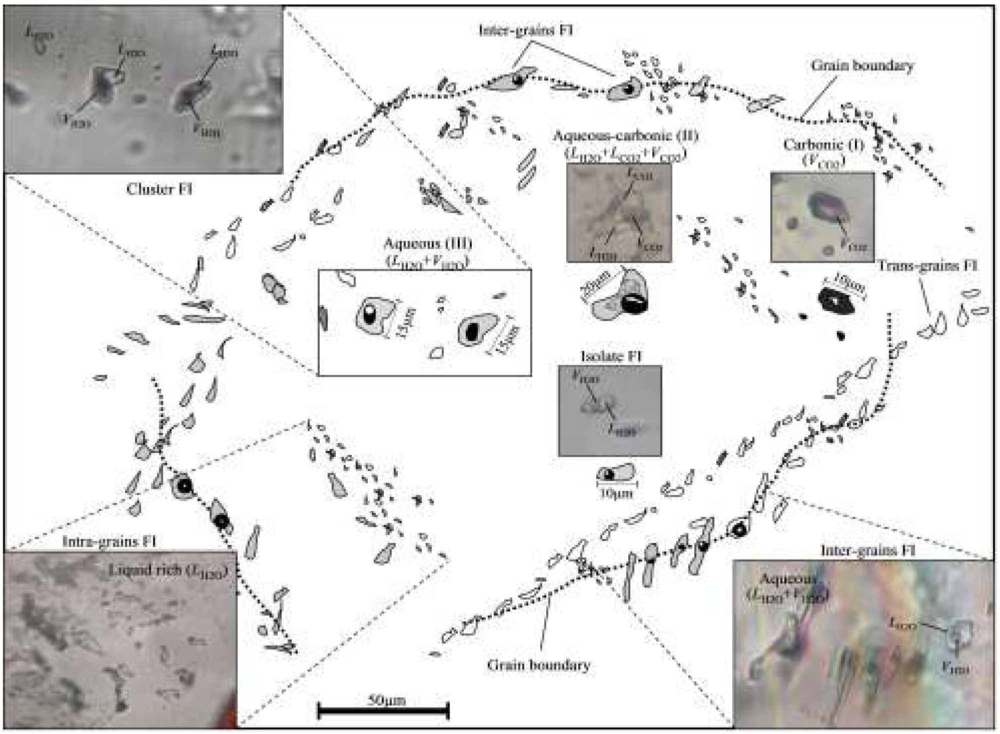

Figure 11: A hand-drawn sketch, based on microscopic observations, shows the distribution of fluid inclusion types in the Muteh deposit. For more details, see the text.

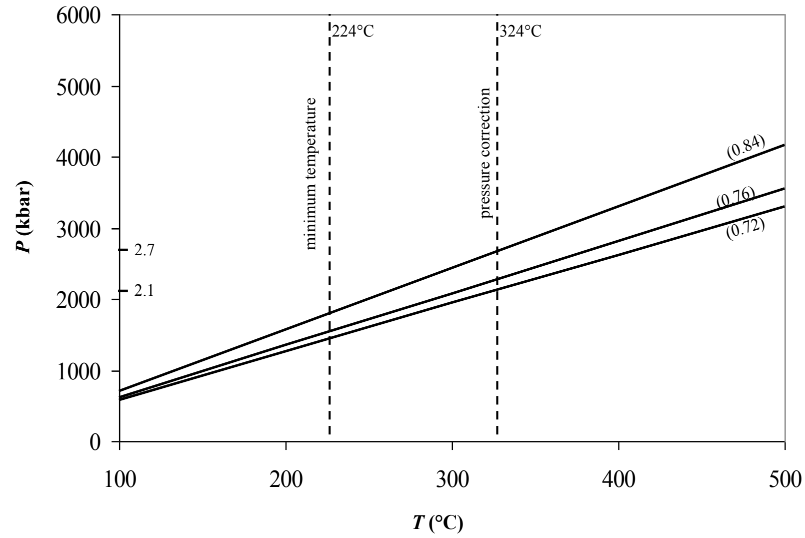

Figure 12: *P-T* diagram with isochores calculated from H_2O-CO_2 inclusions from the Muteh gold deposit. Numbers in parentheses represent the calculated densities of the H_2O-CO_2-NaCl (type2) inclusions. For more details, see the text. After Fan *et al.,* (2003) and Zhang *et al.,* (2005).

Fluid immiscibility

Fluid immiscibility is commonly associated with gold and sulfide deposition in a variety of hydrothermal deposits from Archean to Tertiary age (Yao *et al.,* 2001; Coulibaly *et al.,* 2008). Ramboz *et al.,* (1982) defined four basic criteria for recognizing fluid immiscibility in fluid inclusions. All petrographic and microthermometric data suggest that coexisting types I, II, and III inclusions may have been trapped coevally both as primary and as secondary inclusions. This phenomenon is generally regarded as convincing evidence for fluid immiscibility (Roedder, 1984; Xu and Polland, 1999). As suggested by Hollister (1988, 1990), selective entrapment of CO_2-rich composition from a homogeneous phase CO_2-H_2O fluid following immiscible separation was one of possible mechanism for the formation of CO_2 inclusions (Zhang *et al.,* 2005). All assemblages of primary and secondary inclusions have variable CO_2 contents, composition, density, and homogenization temperatures (Moritz *et al.,* 2006). With attention to coexisting inclusions within the same cluster or along the same microfracture display variations in their properties, the contents of the inclusions reflect either primary. Processes such as heterogeneous trapping of immiscible fluids or secondary processes such as subsequent necking during annealing of microfractures.

Yousefinia (2004) interpreted that the ore fluids of the Muteh mine were associated with boiling and cooling, but several fractures from our study suggest immiscibility as a mechanism responsible for producing the fluids in some inclusions. The aqueous-carbonic inclusions coexist with aqueous and carbonic inclusions either in cluster, isolate or along the same trial and thus are interpreted to have been trapped contemporaneously. The variable range of Tm_{CO2} and Th_{CO2} values for types I and II inclusions is consistent with variable composition and density of these inclusions (this study and Moritz *et al.,* 2006), suggesting that the two inclusion groups resulted from heterogeneous trapping of immiscible fluids (Van Den Kerkhof and Hein., 2001). Fluid immiscibility and/or phase separation will only occur if ambient condition falls below those of the solvus for the respective fluid composition (Zhang *et al.,* 2005). Numerous studies of Hendel and Holister (1981) and Bowers and Helgeson (1983) indicated that CO_2 solubility in the H_2O-CO_2-NaCl system decreases with decreasing temperature and pressure, and also with increasing NaCl. In principle, pressure decrease would lower the CO_2 solubility and result in phase separation and consequent entrapment of CO_2-rich fluids. Inasmuch the post-peak metamorphic formation timing of the auriferous quartz veins investigated in this study, fluid inclusions observed in the veins are clearly related to greenschist-facies retrogression or dehydration of such underthrusted rocks during exhumation of the metamorphic host-rock complex (Moritz *et al.,* 2006). Therefore, the phase separation was most likely caused by a pressure decrease, leading to a drop in temperature through the removal of relatively high enthalpy, low density CO_2-rich fluid (<0.7 g/cm^3) from the system.

Gold transport and deposition

In nature hydrothermal fluids gold is predominantly transported as gold bisulfide (reduced fluid) and chloride (oxygenated fluid) complexes (Shenberger and Barnes, 1989; Hayashi and Ohmoto, 1991; Benning and Seward, 1996; Stefansson and Seward, 2003, 2004; Pal′yanova, 2008). Many previous experimental studies demonstrated that gold is transported as bisulfide complex at low salinities and low fO_2 but at variable pH conditions (Mikucki, 1998; Stefansson and Seward, 2003). The $Au(HS)_2^-$ as a major complex is predominant at near-natural to weakly acidic pH in reduced sulfur-bearing solutions and at relatively low temperatures (Shenberger and Barnes, 1989; Benning and Seward, 1996; Stefansson and Seward, 2003; Tagirov *et al.,* 2005; Pal′yanova, 2008), whereas the $AuHS^0$ and $HAu(HS)_2^0$ complexes are stable at lower pH. The $AuCl^-_2$ complex is predominant in more acidic and high salinity, H_2S^- poor fluids at relatively high fO_2, and at high temperatures. The Muteh Au deposit is similar to many shear zone quartz vein gold deposit formed under comparable temperature and pressure conditions in the greenschist-amphibolite facies terranes. These deposits are commonly characterized by low salinity aqueous-carbonic ore fluids, weakly alkaline to neutral and slightly reducing in most cases (Mikucki and Ridley, 1993; Mikucki, 1998; Zoheir, 2008).

Based on the coexistence of k-feldspar, albite and sericite (muscovite) in auriferous quartz veins at the Muteh Au deposit, the pH of the hydrothermal fluids ranged about from 5 to 6 (Yoo, 2000; Yoo *et al*., 2009). The lack of hematite and highly oxidized minerals and presence of Bismuth and Cu-Bi sulfide phase accompanied with pyrite chalcopyrite and arsenopyrite in the Muteh mine indicates that the hydrothermal fluids were reduced. Also, in the Muteh, the temporal and spatial association of gold with pyrite and chalcopyrite, low salinity fluid inclusions (auriferous forming fluids), the sericite-carbonate alteration assemblage and scarcity of galena and sphalerite sulfide minerals are consistent with conclusion that firstly bisulfide ($Au(HS)^-_2$) and secondary chloride ($AuCl^-_2$) complexes were responsible for gold transport.

Gold deposition from the both bisulfide and chloride complexes may be caused by several mechanisms that include pH changes, fO_2 changes, cooling and dilution, fluid-rock interaction, and fluid unmixing in or along fractures (Broman et al., 1994; Benning and Seward, 1996; Gibert et al., 1998). Changes in fluid pH might have been caused by sericite alteration, which should have added H^+ to the circulation fluid, whereas precipitation of carbonate minerals removed CO_2 from the fluid (e.g., Buchholz *et al.,* 1998). According to Bowers (1991) and Zoheir (2008) effervescence of CO_2 triggered by pressure fluctuations along the shear zone might have also raised both pH and fO_2. Also, sulfidation processes such as pyrite formation in wall-rock, commonly increase fluid fO_2 and reduce fS_2, causing deposition of gold in the quartz veins and wall-rock alteration haloes (bleached zone). According to Mikucki (1998), the heat loss and increase of fO_2 and pH during fluid immiscibility may actually inhibit gold deposition and that only changes in fS_2 would favor gold precipitation at the Muteh.

Ore forming fluid and origin

As aforementioned above, the origin of the fluids at Muteh have a certain trends includes, (1) the low to moderate temperature, highly saline aqueous regional fluids has all the characteristics of basinal brine, typical of evaporite-bearing sedimentary metamorphosed rock units (e.g., Rich, 1979; Mora and Valley, 1989; Oliver *et al.,* 1992; Giuliani *et al.,* 1995); (2) the high to moderate temperature, low salinity aqueous fluid and the H_2O-CO_2-bearing ore forming fluids, typical of the majority of Archean and Phanerozoic mesothermal quartz vein style gold deposits in greenschist-facies terranes (Gebre-Mariam *et al.,* 1995; McCuaig and Kerrich, 1998; Yao *et al.,* 1999; Kolb and Meyer, 2002; Zhang *et al.,* 2003b) that fluids was generated as a consequence of the metamorphic dehydration/decarbonation processes which could have escaped along the extensional structural setting (e.g., normal faults) during exhumation of the metamorphic host-rock complex at Muteh. Such typical ore fluids includes low salinity, low CO_2 content aqueous fluids are typical for both orogenic and intrusion-related gold deposits (Ridley and Diamond, 2000; Lang and Baker, 2001; Baker, 2002; Yoo *et al.,* 2009). Although metamorphic components have predominantly been proposed for the fluid source for those types of deposits (Goldfarb *et al.,* 1998; Witt *et al.,* 1997), the roles of magmatic source and evolved meteoric waters have also been proposed for the green-schist or sub-amphibolite facies deposits (Burrows and Spooner, 1987; Cameron and Hattori, 1987; Yao *et al.,* 1999; Zhang *et al.,* 2003b).

At the Muteh Au deposit, a direct link between metamorphism of the host rocks and ore formation as suggested by Paidar-Saravi (1989), but according to $^{40}Ar/^{39}Ar$ data of Moritz *et al.,* (2006) the regional metamorphic fluids are not a viable source. Moritz *et al.,* (2006) suggested that the gold ore formation at Muteh was early to middle Eocene in age and significantly (about 40 m.y. or more) younger than the metamorphic basement in the area. Instead, the close temporal and spatial association between mineralization zone and the granite-granodiorite suggests that deep-crustal granitic devolatilization would have generated the mineralizing fluids. Moritz *et al.,* (2006) considered that the Eocene granodiorite intrusion emplaced in the westernmost metamorphic complex (Fig. 2) is coeval with the formation of the gold deposit at Muteh. Such genetic association between magmas and hydrothermal ore deposit has been documented in scores of geological studies of mineralization close to magmatic intrusions (e.g., Nabelek and Ternes, 1997; Jiang *et al.,* 1999; Yao *et al.,* 1999; Zhang *et al.,* 2005). Meteoric waters seem to be another likely fluid source for the Muteh deposit (Abdollahi *et al.,* 2007), as downward-percolating meteoric water is commonly reported to be a late saline, low temperature aqueous fluid that have circulated in the metamorphic complex after or during the latest stages of gold ore formation.

As discussed above and studies of Moritz *et al.,* (2006) and Abdollahi *et al.,* (2007) concluded that the ore-forming fluids in the Muteh gold mine may be a mixture of meteoric water and magmatic water.

Comparison of Muteh deposit with orogenic and intrusion-related Au-deposits (reduced granitic intrusions)

Knowledge of the timing of mineralization relative to tectonic, metamorphic, and magmatic events is fundamental for understanding the genesis of mineral deposits (Yang *et al.,* 2003). Present, gold deposit of different crustal levels have been classified as epithermal, intrusion-related, or thermal aureole gold (TAG), and orogenic, reflecting interest in the relationship between mineral deposits and their tectonic setting (Robert *et al.,* 1997; Groves *et al.,* 2005; Poulsen *et al.,* 2000; Lang and Baker, 2001; Baker, 2005; Wall, 2005). According to Yoo *et al.,* (2009) use of the term "*intrusion-related*" for a specific ore deposit model (e.g., Thompson *et al.,* 1999; Lang and Baker, 2001) has resulted in semantic difficulties in discussing the genetic relationships of deposits, as some deposits, despite having demonstrated spatial, temporal, and/or genetic relationships with intrusions, may not fit the intrusion-related model.

Quartz veins mineralization style of the Muteh mine have many features in common with deposits of orogenic type includes, (1) metapelite country rocks, (2) low sulfidation style of the ore mineral assemblage (arsenopyrite and pyrite), (3) sericite-carbonate alteration, and (4) low salinity aqueous-carbonic ore fluids, and diagnostic features of intrusion-related gold deposits are; (1) metaluminous, subalkalic intrusions of intermediate to felsic composition that linear the boundary between ilmenite and magnetite series, (2) carbonic hydrothermal fluids, (3) a metal assemblage that variably combines gold with elevated Bi, As, Te, and/or Sb and low concentrations of base metals (except chalcopyrite), (4) a low sulfide mineral content, mostly <5 vol%, with a reduced ore mineral assemblage that typically comprises Cu-Bi sulfide, arsenopyrite, pyrrhotite, and pyrite and which to some extent lacks of magnetite or hematite, (5) spatial and temporal associatin with magmatism (Thiele *et al.,* 1968; Samani, 1988; Rashidnejad-Omran *et al.,* 2002; Moritz *et al.,* 2006), and (6) wide range in P-T conditions that span brittle and ductile regimes in mineralization.

According to Hart and Goldfarb (2005) and Goldfarb *et al.,* (2005) the orogenic and intrusion-related gold deposits have many similar features such as reduced sulfide assemblages, gangue mineralogy, metal associations, low salinity, CO_2-bearing fluids, post-peak metamorphic lode, spatial and temporal association with granitoids and local structural controls that mostly result from their formation from fluids with similar compositions and their formation in setting that host large amounts of felsic magma. Furthermore, the extensional structural setting during exhumation/ dehydration of the metamorphic host-rock complex and gold ore formation in the conjugate normal fault system at Muteh is a clearly distinct feature, which significantly differs from the majority of orogenic gold deposits, where orebodies are typically hosted by reverse component shear zones, which were formed during a main phase of crustal shortening in transspressional to compressional tectonic setting (Groves *et al.,* 2003; Goldfarb *et al.,* 2005; Moritz *et al.,* 2006). Also, according to Lang and Baker (2001) mineral deposits in intrusion-related gold systems span a broad range in style and deposition relative to intrusive centers.

McCoy *et al.,* (1997), Thompson *et al.,* (1999), Hart *et al.,* (2000), and Lang *et al.,* (2000) have described the more common patterns of zoning in the intrusion-related systems which based on ore mineralogy, alteration and metal distribution to some extent observed at Muteh gold deposit. According to Hart *et al.,* (2000) intrusion-related gold deposits, separated into proximal and distal deposits based on their relationship to intrusions. Intrusion-hosted or proximal deposits comprise auriferous, mostly sheeted and lesser stockwork vein deposits located in host rock adjacent to the intrusions, or slightly removed from them and characterized by metal assemblages of Au-Bi±Te±As±Mo±W (Hart *et al.,* 2000; Lang and Baker, 2001). Also, distal deposits are located beyond the intrusive-hosted setting and the outer limite of metamorphic aureole are includes auriferous, mesothermal to epithermal quartz-sulfide veins along steep faults (e.g., Donlin Creek, Alaska; Ebert *et al.,* 1998) with typical metal signature of Au-As-Sb±Hg and veins enriched in Ag±Au. Vertical variation in distal deposit style are less well characterized, but include differences in the relative importance of ductile and brittle shear zones, the degree of lateral dispersion or concentration of hydrothermal fluids, metal signatures, and the composition of hydrothermal fluids (e.g., Lang *et al.,* 2000; Lang and Baker, 2001).

Our study shows that at Muteh ore deposit, Chah-Khatoon, Senjedeh and Cheshmeh-Gowhar gold deposits characterized by ore mineralogy comprises a complex suite of tellurium- and bismuth-bearing minerals (e.g., emplectite), native gold, electrum, sulfosalts and, sulfides that are consistent with strongly to moderately reduced conditions (McCoy *et al.,* 1997), occurrence of feldspatic alteration, dominated by albite and and/or k-feldspar associated with orebodies (Fig. 8) and metal assemblages of Au-Bi±Te±As that characteristic of intrusion-hosted or proximal setting of intrusion-related gold systems.

Furthermore, in the Chah-Bagh gold deposit absence of Au-Bi±Te metal assemblages and tellurium- and bismuth bearing minerals, and instead occurrences of Au-As-Ag±Sb metal assemblages dominated by Cu-bearing arsenopyrite, As-bearing pyrite, and native silver in ductile to brittle shear zone (Kouhestani, 2005; Kouhestani *et al.,* 2005) located beyond the other deposits in the Muteh mine area, indicated that gold mineralization in the Chah-Bagh and Tangeh-Zar (Fig. 2) deposits lesser or more similar to distal deposits of intrusion-related gold systems define by Hart *et al.,* (2000) and Lang and Baker, (2001) (Fig. 13).

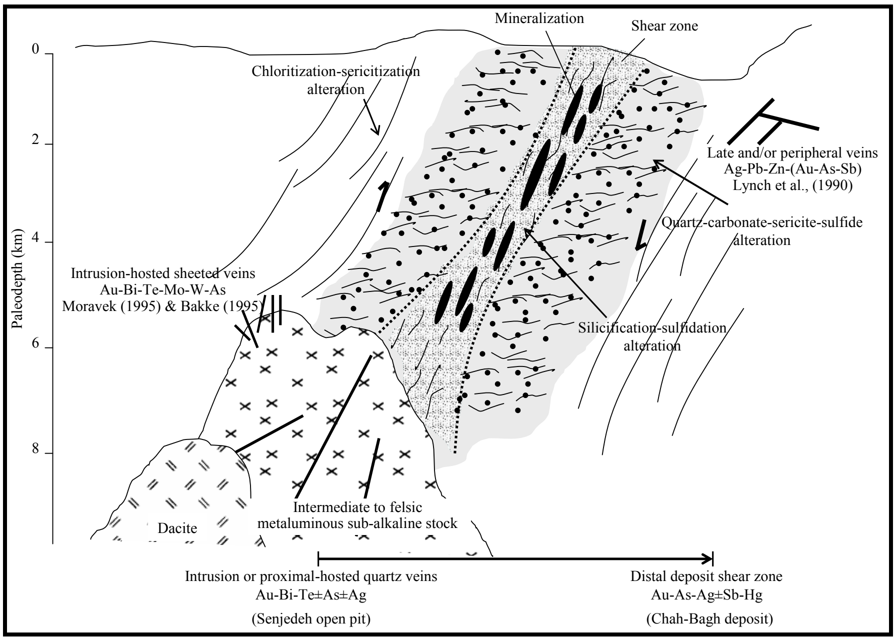

Figure 13. Schematic geological cross section of the Muteh gold mine, emphasizing the vertical and lateral variation in deposit style, alteration characteristics, metal distribution, and field and petrographic observations. According to model of Hart *et al.,* (2000) and Lang and Baker, (2001).

Thus, given such genetic linkage between tectonic evolution of lithospheric mantle through upper crust with the tectono-magmatic history of Sanandaj-Sirjan zone (SSZ) in Tertiary accompanied with exhumation of the metamorphic host-rock complex (early to middle Eocene time) due to extensional structure setting, and possibly local magmatism during the late stages of the Zagros orogeny within the Neotethys Eurasian metallogenic belt (Mohajjel *et al.,* 2003; Golonka, 2004; Azizi and Moinevaziri, 2009), the Muteh deposit can be favored as an granite-related Au-deposit more plausible than orogenic gold deposit in the sense of Groves *et al.,* (2003) and Goldfarb *et al.,* (2005). Nonetheless, with attention to whole evidence are mentioned this paper we believe that the study in this field must be continue.

Conclusions

The Muteh gold deposit is mainly hosted by metarhyolite, biotite-plagioclase gneiss and quartz-sericite schist. All host rocks have been strongly fractured and sheared, variying from incipient mylonite and mylonite to ultra-mylonite.

The distribution and mineralization of the Muteh gold deposit are structurally, controlled by ductile to brittle shear zones and related to intrusive bodies in the area. Like most this gold deposit in the world, the shear zone provided conduits for transport of Au-bearing fluids and structural sites for deposition of gold and other metals, especially, the conjugate of two episodes of faults and shear zones favor the occuration of gold mineralization.

At Muteh, gold mineralization is closely associated with intense silicious hydrothermal alteration mainly controlled by shear zones, with a typical greenschist-sub amphibolite facies alteration assemblages of sericite+ albite+ k-feldspar+ chlorite+ carbonate+ quartz+ biotite. Hydrothermal alteration is pervasive in the wallrock greenschist and granite including sericitization, chloritization, carbonatization and minor kaolinization.

Two types auriferous quartz veins recognized at

Muteh deposit that separated by mineralogy-style, textures, fracture and faulting events. Type I quartz veins contain pyrite, chalcopyrite, Cu-Bi sulfide (emplectite), arsenopyrite, pyrrhotite, native gold and marcasite with albite, k-feldspar, zircon, and rutile as gangue minerals occurred within a conjugate NW-trending normal dextral fault system. Type II quartz-pyrite-carbonate veins accompanied with silicified highly-deformed mylonite and ultramylonite rocks and extend in a N40-50W direction in opposite dipping.

Fluid inclusion petrography and microthermometric results suggest that three types of fluid inclusions are present in the Muteh. Type 1 carbonic inclusions have homogenization temperatures of CO_2 between 12.6°C to 22.3°C. Type 2 aqueous-carbonic inclusions shows salinities of 2.3-12.5 wt.% NaCl eq. and Th_{total} of 145.6°C to 304.2°C. Type 3 aqueous inclusions includes two groups, type 3a inter-grain to trans-grain trial-bound inclusions have salinity of 2.1-15.2 wt.% NaCl eq. and Th_{total} of 212.2°C to 297.6°C from auriferous quartz-sulfide veins, and type 3b inter-grain to intra-grain trials inclusions shows salinities of 16.4-28.2 wt.% NaCl eq. and Th_{total} between 147.4°C to 245.6°C belongs to regional or barren quartz veins.

Evidences of metaluminous, subalkalic granitoid intrusive rocks, alteration assemblages dominated by albite and/or k-feldspar associated with orebodies, low sulfide ore mineralogy content, metal distributions of Au-Bi±Te±As that are consistent with strongly to moderately reduced conditions, presence of carbonic hydrothermal fluids and genetic linkage between tectono-magmatic history of Sanandaj-Sirjan zone (SSZ) in Tertiary accompanied with occurrence of magmatism during the late stages of the Zagros orogeny, shows that gold mineralization in the Muteh, lesser or more similar to intrusion-related gold systems define by Hart *et al.,* (2000) and Lang and Baker, (2001).

References

Abdollahi, M.J., Karimpour, M.H., Kheradmand, A., 2007. O-H and S stable isotopes in the Muteh gold deposit, Golpaygan area, Isfahan, Iran. Geological Survey of Iran, Geology Symposium, 26rd, Tehran, Iran, p. 60–71 (Persian and English abs.).

Alavi, M., 1994. Tectonics of the Zagros orogenic belt of Iran: New data and interpretations. Tectonophysics 229, 211–238.

Alavi, M., 2004. Regional stratigraphy of the Zagros fold-thrust belt of Iran and its proforeland evolution. American Journal of Science 304, 1–20.

Aliyari, F., Rastad, E., Mohajjel, M., Arehart, G.B., 2009. Geology and geochemistry of D-O-C isotope systematics of the Qolqoleh gold deposit, Northwestern Iran: Implication for ore genesis. Ore Geology Review (article in press).

Azizi, H., Moinevaziri, H., 2009. Review of the tectonic setting of Cretaceous to Quaternary volcanism in northwestern Iran. Journal of Geodynamics (article in press).

Baker, T., 2002. Emplacement depth and carbon dioxide-rich fluid inclusions in intrusion-related gold deposits. Economic Geology, 97, 1111–1117.

Baker, T., 2005. New constraints on the chemistry of magmas and fluids associated with intrusion-related gold deposits. New Zealand Minerals Conference Proceedings, pp 56–64.

Bakke, A.A., 1995. The Fort Knox "porphyry" gold deposit: structurally controlled stockwork and shear quartz vein, sulfide-poor mineralization hosted by a Late Cretaceous pluton, east-central Alaska. Can Inst Min Metall Spec 46, 795-802.

Benning, L.G., Seward, T.M., 1996. Hydrosulphide complexing of Au(I) in hydrothermal solutions from 150–400°C and 500–1500 bars. Geochim Cosmochim Acta 60, 1849–1871.

Bodnar, R.J., 2003. Introduction to aqueous-electrolyte fluid inclusions. Mineralogical Association of Canada Short Course 32, 81–100.

Bowers, T.S., Helgeson, H.C., 1983. Calculation of the thermodynamic and geochemical consequences of nonideal mixing in the system H_2O–CO_2–NaCl on phase relations in geologic systems: equation of state for H_2O–CO_2–NaCl fluids at high pressures and temperatures. Geochim Cosmochim Acta 47, 1247–1275.

Bowers, T.S., 1991. The deposition of gold and other metals: pressure induced fluid immiscibility and associated stable isotope signatures. Geochim Cosmochim Acta 55, 2427–2434.

Broman, C., Billström, K., Gustavsson, K., Fallick, A.E., 1994. Fluid inclusions, stable isotopes and gold deposition at Björkdal, northern Sweden. Mineralium Deposita 29, 139–149.

Brown, P.E., 1989. FLINCOR: a microcomputer program for the reduction and investigation of fluid inclusion data. American Mineralogist 74, 1390–1393.

Brown, P.E., Hagemann, S.G., 1995. MacFlincor and its application to fluids in Archean lode-gold deposits. Geochimica et Cosmochima Acta 59, 3943–3952.

Buchholz, P., Herzig, P., Friedrich, G., Frei, R., 1998. Granite-hosted gold mineralisation in the Midlands greenstone belt: a new type of low-grade large scale gold deposit in Zimbabwe. Mineralium Deposita 33, 437–460.

Burrows, D.R., Spooner, E.T.C., 1987. Generation of a magmatic H_2O–CO_2 fluid enriched in Mo, Au, and W within an Archean sodic granodiorite stack, Mink Lake, Northwestern Ontario. Economic Geology 82, 1931–1957.

Burruss, R.C., 1981. Analysis of phase equilibria in C–O–H–S fluid inclusions. Mineralogical Association of Canada Short Course Handbook 6, 39–74.

Cameron, E.M., Hattori, K., 1987. Archean gold mineralization and oxidized hydrothermal fluids. Economic Geology 82, 1177–1191.

Coulibaly, Y., Boiron, M.C., Cathelineau, M., Kouamelan, A.N., 2008. Fluid immiscibility and gold deposition in the Birimian quartz veins of the Angovia deposit (Yaoure, Ivory Coast). Journal of African Earth Science 50, 234–254.

Cox, S.F., Sun, S.S., Etheridge, M.A., Wall, V.J., Potter, T.F., 1995. Structural and geochemical controls on the development of turbidite-hosted gold quartz vein deposits, Wattle Gully mine, central Victoria, Australia. Econpmic Geology 90, 1722–1746.

Diamond, L.W., 1992. Stability of CO_2 clathrate hydrate + CO_2 liquid + CO_2 vapour + aqueous KCl-NaCl solutions: Experimental determinations and application to salinity estimates of fluid inclusions. Geochimica et Cosmochimica Acta, 56, 273–280.

Fan, H., Zhai, M., Xie, Y., Yang, J., 2003. Ore-forming fluids associated with granite-hosted gold mineralization at the Sanshandao deposit, Jiaodong gold province, China. Mineralium Deposita 38, 739–750.

Farhangi, A., 1991. Gold prospecting in Muteh region, Esfahan, Iran, in Ladeira, E.A., ed., Brazil Gold '91: Rotterdam, Balkema, p. 801–804.

Gebre-Mariam, M., Hagemann, S.G., Groves, D.I., 1995. A classification scheme for epigenetic lode-gold deposits. Mineralium Deposita 30, 408–410.

Ghasemi, A., Talbot, C.J., 2005. A new tectonic scenario for the Sanandaj–Sirjan Zone (Iran). Journal of Asian Earth Sciences 24, 1–11.

Gibert, F., Pascal, M.L., Pichavant, M., 1998. Gold solubility and speciation in hydrothermal solutions: experimental study of the stability of hydrosulphide complex of gold (AuHSo) at 350 to 450°C and 500 bars. Geochim Cosmochim Acta 62, 2931–2947.

Giuliani, G., Cheilletz, A., Arboleda, C., Carillo, V., Rueda, F., Baker, J., 1995. An evaporitic origin of the parent brines of the Colombian emeralds: Fluid inclusions and sulfur isotopes evidence. European Journal of Mineralogy 7, 151–165.

Goldfarb, R., Phillips, G.N., Nokleberg, W.J., 1998. Tectonic setting of synorogenic gold deposit of the Pacific Rim. Ore Geology Reviews 13, 185–218.

Goldfarb, R.J., Baker, T., Dube, B., Groves, D.I., Hart, C.J.R., Gosselin, P., 2005. Distribution, character, and genesis of gold deposits in metamorphic terranes. In: Hedenquist JW, Thompson, J.F.H., Goldfarb, R.J., Richards, J.P., (eds). Economic Geology 100th Anniversary Volume, pp 407–450.

Golonka, J., 2004. Plate tectonic evolution of the southern margin of Eurasia in the Mesozoic and Cenozoic. Tectonophysics 381, 235–273.

Groves, D.I., Condie, K.C., Goldfarb, R.J., Hronsky, J.M.A., Vielreicher, R.M., 2005. Secular changes in global tectonic processes and their influence on the temporal distribution of gold-bearing mineral deposits. Economic Geology 100, 203–224.

Haghipour, A.A., Aghanabati, S.A., 1985. Geological map of Iran, Geol. Surv. Iran.

Hajizadeh, M., 2009. Spatial distribution of gold mineralization in the Muteh district and the role of tectonic controls in this distribution, Unpublished M.Sc. thesis, Tehran, Iran, University of Tarbiat Moallem, 110 p. (in Persian).

Hart, C.J.R., Goldfarb, R.J., 2005. Distinguishing intrusion-related from orogenic gold systems. New Zealand Minerals Conference Proceedings, pp 125–133.

Hayashi. K., Ohmoto, H., 1991. Solubility of gold in NaCl- and H_2S bearing aqueous solutions at 250–350°C. Geochim Cosmochim Acta 55, 2111–2126.

Hendel, E.M., Hollister, L.S., 1981. An empirical solvus for CO_2–H_2O–2.6 wt.% salt. Geochimica et Cosmochimica Acta 45, 225–228.

Hollister, L.S., 1988. On the origin of CO_2-rich fluid inclusions in migmatites. Journal of Metamorphic Geology 6, 467–474.

Hollister, L.S., 1990. Enrichment of CO_2 in fluid inclusions in quartz by removal of H_2O during crystal plastic deformation. Journal of Structural Geology 12, 895–901.

Jankovic, S., 1977. The copper deposits and geotectonic setting of the Tethyan Eurasian metallogenic belt. Mineralium Deposita, 12, 37–47.

Jankovic, S., 1997. The Carpatho-Balkanides and adjacent area: A sector of the Tethyan Eurasian metallogenic belt. Mineralium Deposita, 32, 426–433.

Jiang, N., Xu, J., Song, M., 1999. Fluid inclusion characteristics of mesothermal gold deposits in the Xiaoqinling district, Shaanxi and Henan Provinces, People's Republic of China. Mineralium Deposita 34, 150–162.

Kolb, J., Meyer, F.M., 2002. Fluid inclusion record of the hypozonal orogenic Renco gold deposit (Zimbabwe) during the retrograde P–T evolution. Contributions to Mineralogy and Petrology 143, 495– 509.

Kouhestani, H., 2005. Geology, mineralogy, geochemistry and fabrics of gold mineralization in Chah-Bagh shear zones at Muteh mining area (southwest of Delijan, Esfahan province): Unpublished M.Sc. thesis, Tehran, Iran, University of Tarbiat-Modarres, 222 p. (in Persian).

Kouhestani, H., Rastad, E., Rasidnejad, N., and Mohajjel, M., 2005. The role of deformation and alteration in gold mineralization in Chah-Bagh deposit shear zones [abs.]: Geological Survey of Iran, Geology Symposium, 23rd, Tehran, Iran, p. 50–51 (Persian and English abs.).

Kranz R.L., 1983. Microcracks in rocks: a review. Tectonophysics 100 (1–3), 449–480. Van den Kerkhof A.M., Hein U.F., 2001. Fluid inclusion petrography. Lithos 55, 27–47.

Lang, J.R., Baker, T., 2001. Intrusion-related gold systems: the present level of understanding. Mineralium Deposita 36, 477–489.

Lynch G.J.V., Longstaffe, F.J., Nesbitt, B.E., 1990. stable isotopic and fluid inclusion indications of larg-scale hydrothermal paleo-flow, boiling and fluid mixing in the Keno Hill Ag-Pb-Zn district, Yukon Territory, Canada. Geochim Cosmochim Acta 54, 1045-1059.

McCuaig, T.C., Kerrich, R., 1998. P–T–t-deformation-fluid characteristics of lode gold deposits: evidence from alteration systematics. Ore Geology Reviews 12, 381–453.

McCoy, D., Newberry, R.J., Layer, P., DiMarchi, J.J., Bakke, A., Mas-terman, S., Minehane, D.L., 1997. Plutonic-related gold deposits of Interior Alaska. In: Goldfarb, R.J., Miller, L.D., (eds) Mineral deposits of Alaska. Economic Geology 9, 191-241.

Mikucki, E.J., Ridley, J.R., 1993. The hydrothermal fluid of Archaean lode–gold deposits at different metamorphic grades: compositional constraints from ore and wall rock alteration assemblages. Mineralium Deposita 28, 469–481.

Mikucki, E.J., 1998. Hydrothermal transport and depositional processes in Archaean lode-gold systems: a review. Ore Geol Rev 13, 307–321.

Mohajjel, M., Fergusson, C.L., 2000. Dextral transpression in late cretaceous continental collision, Sanandaj–Sirjan Zone, Western Iran. Journal of Structural Geology 22, 1125–1139.

Mohajjel, M., Fergusson, C.L., Sahandi, M.R., 2003. Cretaceous–Tertiary convergence and continental collision, Sanandaj–Sirjan Zone, Western Iran. Journal of Asian Earth Sciences 21, 397–412.

Mora, C.I., Valley, J.W., 1989. Halogen-rich scapolite and biotite—implications for metamorphic fluid rock interaction. American Mineralogist 74, 721–37.

Moravek, P., 1995. The Mokrsko gold deposit. In: Moravek P (ed) Gold deposit of the central and SW part of the Bohemian Massive. 3rd Biennial SGA meeting, pp: 33-61.

Moritz, R., Ghazban, F., Singer, B.S., 2006. Eocene gold ore formation at Muteh, Sanandaj-Sirjan tectonic zone, western Iran: a result of late-stage extension and exhumation of metamorphic basement rocks within the Zagros orogen. Economic geology 101, 1497-1524.

Nabelek, P.I., Ternes, K., 1997. Fluid inclusions in the Harney Peak Granite, Black Hills, south Dakota, USA: implications for solubility and evolution of magmatic volatiles and crystallization of leucogranite magmas. Geochimica et Cosmochimica Acta 61, 1447–1465.

Oliver, N.H.S., Wall, V.J., Cartwright, I., 1992. Internal control of fluid compositions in amphibolite-facies scapolitic calc-silicates, Mary-Kathleen, Australia. Contributions to Mineralogy and Petrology 111, 94–112.

Pal′yanova, G., 2008. Physicochemical modeling of the coupled behavior of gold and silver in hydrothermal processes: gold fineness, Au/Ag ratios and their possible implications. Chemical geology 255, 399-413.

Paidar-Saravi, H., 1989. Petrographisch-lagerstättenkundliche Untersuchungen an goldführenden Gesteinen im Muteh-Gebiet im Westen vom Zentraliran: Heidelberger Geowissenschaftliche Abhandlungen 33, 174 p.

Potter, R.W. II, Clynne, M.A., Brown, D.L., 1978. Freezing point depression of aqueous sodium chloride solutions. Economic Geology 73, 284–285.

Poulsen, K.H., Robert, F., Dube, B., 2000. Geological classification of Canadian gold deposits. Geological survey of Canada, Bulletin 540, 106.

Rachidnejad-Omran N., Emami, M.H., Sabzehei, M., Rastad, E., Bellon, H., and Piqué, A., 2002. Lithostratigraphie et histoire paléozoïque à paléocène des complexes métamorphiques de la région de Muteh, zone de Sanandaj-Sirjan (Iran méridional). Comptes rendus Geoscience 334, 1185–1191.

Ramboz, C., Pichavant, M., Weisbrod, A., 1982. Fluid immiscibility in natural processes: use and misuse of fluid inclusion data. II. Interpretation of fluid inclusion data in terms of immiscibility. Chemical Geology 37, 29–48.

Rich, R.A., 1979. Fluid inclusion evidence for Silurian evaporites in southeastern Vermont: Summary. Geological Society of America Bulletin 90, 901–902.

Ridley, J.R., Diamond, L.W., 2000. Fluid chemistry of orogenic lode gold deposits and implications for genetic models. Reviews in Economic Geology 13, 141–162.

Robert, F., Kelly, W.C., 1987. Ore-forming fluids in Archean goldbearing quartz veins at the Sigma Mine, Abitibi greenstone belt, Quebec, Canada. Economic Geology 82, 1464–1482.

Robert, F., Poulsen, K.H., Dube, B., 1997. Gold deposits and their geological classification. Exploration 97, April 1997, Toronto, Canada, pp 209–219.

Roedder, E., Bodnar, R.J., 1980. Geological pressure determinations from fluid inclusions studies. Annual Review of Earth and Planetary Sciences 8, 263–301.

Roedder, E., 1984. Fluid inclusions. Reviews in Mineralogy 12 (644 pp.)

Samani, B.A., 1988. Metallogeny of the Precambrian in Iran. Precambrian Research 39, 85–106.

Schmidt Mumm, A., Oberthür, T., Vetter, U., Blenkinsop, T.G., 1997. High CO_2 content of fluid inclusions in gold mineralisations in the Ashanti Belt, Ghana: a new category of ore forming fluids? Mineralium Deposita 3, 107–118.

Shenberger, D.M., Barnes, H.L., 1989. Solubility of gold in aqueous sulphide solutions from 150 to 350°C. Geochim Cosmochim Acta 53, 269–278.

Shepherd, T.J., Rankin, A.H., Alderton, D.H.M., 1985. A Practical Guide to Fluid Inclusion Studies. Blackie and Son, 239 pp.

Sibson, R.H., 1987. Earthquake rupturing as a mineralizing agent in hydrothermal systems. Geology 15, 701–704.

Simmons, G., Richter, D., 1976. Microcracks in rocks. In: Strens RGJ (ed) The physics and chemistry of minerals and rocks. Wiley, Toronto, pp 105–137.

Stefansson, A., Seward, T.M., 2003. Stability of chloridogold(I) complexes in aqueous solutions from 300 to 600°C and from 500 to 1800 bar. Geochim Cosmochim Acta 67, 4559–4576.

Stefansson, A., Seward, T.M., 2004. Gold (I) complexing in aqueous sulphide solutions to 500°C at 500 bar. Geochim Cosmochim Acta 68, 4121–4143.

Tagirov, B.R., Salvi, S., Schott, J., Baranova, N., 2005. Experimental study of gold-hydrosulphide complexing in aqueous solutions at 350–500°C, 500 and 1000 bars using mineral buffers. Geochim Cosmochim Acta 69, 2119–2132.

Thiele, O., Alavi, M., Assefi, R., Hushmand-zadeh, A., Seyed-Emami, K., Zahedi, M., 1968. Explanatory text of the Golpaygan quadrangle map 1:250,000: Geological Survey of Iran, Geological Quadrangle E7, 24 p.

Thompson, JF.H., Sillitoe, R.H., Baker, T., Lang, J.R., Mortensen, J.K., 1999. Intrusion-related gold deposits associated with tungsten–tin provinces. Mineralium Deposita 34, 323–334.

Touret, J.L.R., 1981. Fluid inclusions in high grade metamorphic rocks. In: Hollister L, Crawford ML (eds) Short course in fluid inclusions: applications to petrology. Mineralogical Association of Canada, Calgary, pp 182–208.

Wall, V.J., 2005. TAG: thermal aureole (pluton-related) gold systems. Australian Institute of Geoscientists. Quarterly Newsletter 79, 1–7.

Witt, W.K., Knight, J.T., Mikucki, E.J., 1997. A synmetamorphic lateral Southern Kalgoorlie and Norseman Terranes, Western Australia. Economic Geology 92, 407–437.

Xu, G., Pollard, P.J., 1999. Origin of CO_2-rich fluid inclusions in syn-orogenic veins from the Eastern Mount Isa Fold Belt, NW Queensland, and their implications for mineralization. Mineralium Deposita 34, 395–404.

Yang, J., Wu, F., Wilde, S.A., 2003. A review of the geodynamic setting of large-scale late Mesozoic gold mineralization in the North China Craton: an association with lithospheric thinning. Ore Geology Reviews 23, 125–152.

Yao, Y., Morteani, G., Trumbell, R.B., 1999. Fluid inclusions microthermometry and the P–T evolution of gold-bearing hydrothermal fluids in the Niuxinshan gold deposit, eastern Hebei Province, NE China. Mineralium Deposita 34, 348–365.

Yao, Y., Murphy, P.J., Robb, L.J., 2001. Fluid characteristics of granitoid hosted gold deposits in the Birimian Terrane of Ghana: a fluid inclusion microthermometric and Raman spectroscopic study. Economic Geology 96, 1611–1643.

Yoo, B.C., 2000. Mineralogy and geochemical study of some mesothermal gold–silver-bearing vein deposits in the Yugu-Kwangchun mine district, Republic of Korea. PhD thesis, Chungnam National University.

Yoo, B.C., Lee, K.H., White, C.N., 2009. Mineralogical, fluid inclusion, and stable isotope constraints on mechanisms of ore deposition at the Samgwang mine (Republic of Korea)-a mesothermal, vein-hosted gold–silver deposit, Mineralium Deposita, published online.

Yousefinia. N., 2004. Fluid inclusion studies of the Muteh gold deposit and their implication as an exploration factor for recognition auriferous and barren zones, Unpublished M.Sc. thesis, Tehran, Iran, University of Tarbiat Moallem, 130 p. (in Persian).

Zhang, Y.G., Frantz, J.D., 1987. Determination of the homogenization temperatures and densities of supercritical fluids in the system NaCl–KCl–$CaCl_2$ –H_2O using synthetic fluid inclusions. Chemical Geology 64, 335–350.

Zhang, L., Liu, T., Shen, Y., Zeng, Q., Li, G., 2003b. Structure, Isotopes, and 40Ar/39Ar dating of the Pengjiakuang gold deposit, Mesozoic Jiaolai Basin, Eastern China. International Geology Review 23, 71–90.

Zhang, X.H., Liu, Q., Ma, Y.J., Wang, H., 2005. Geology, fluid inclusions, isotope geochemistry, and geochronology of the Paishanlou shear zone-hosted Gold Deposit, North China Craton. Ore Geology Reviews 26, 325–348.

Zoheir, B.A., 2008. Structural controls, temperature–pressure conditions and fluid evolution of orogenic gold mineralization at the Betam mine, south Eastern Desert, Egypt. Mineralium Deposita 43, 79–95.